Realia et naturalia

DISSERTATIONES
GEOLOGICAE
UNIVERSITATIS
TARTUENSIS
39

LAURI JOOSU

Petrography and the rare earth element composition of apatite in 2 Ga Onega and Pechenga basins, Russia: the environmental settings for phosphogenesis

TARTU ÜLIKOOL · UNIVERSITAS TARTUENSIS · 1632

DISSERTATIONES GEOLOGICAE UNIVERSITATIS TARTUENSIS
39

DISSERTATIONES GEOLOGICAE UNIVERSITATIS TARTUENSIS
39

LAURI JOOSU

Petrography and the rare earth element composition of apatite in 2 Ga Onega and Pechenga basins, Russia: the environmental settings for phosphogenesis

UNIVERSITY OF TARTU
PRESS
1632

Department of Geology, Institute of Ecology and Earth Sciences, Faculty of Science and Technology, University of Tartu, Estonia.

This dissertation is accepted for the commencement of the degree of Doctor of Philosophy in Geology at the University of Tartu on the 15th of June 2015 by the Scientific Council of the Institute of Ecology and Earth Sciences, University of Tartu.

Supervisors: Aivo Lepland, Norwegian Geological Survey, Norway
Kalle Kirsimäe, Department of Geology, University of Tartu, Estonia

Opponent: Prof. Juha Karhu, Department of Geosciences and Geography, University of Helsinki

This thesis will be defended at the University of Tartu, Estonia, Chemicum, Ravila 14A, room 1019, on the 26th of August 2015 at 12:15.

Publication of this thesis is granted by the Institute of Ecology and Earth Sciences, University of Tartu and by the Doctoral School of Earth Sciences and Ecology created under the auspices of the European Social Fund.

ISSN 1406-2658
ISBN 978-9949-32-891-8 (print)
ISBN 978-9949-32-892-5 (pdf)

University of Tartu Press
www.tyk.ee

CONTENTS

LIST OF ORIGINAL PUBLICATIONS

This thesis is based on the following published papers, which are referred to in the text by their Roman numerals. The papers are reprinted by kind permission of the publishers.

I **Joosu, L.**, Lepland, A., Kirsimäe, K., Romashkin, A.E., Roberts, N.M.W., Martin, A.P., Črne, A.E. (2015) The REE-composition and petrography of apatite in 2 Ga Zaonega Formation, Russia: The environmental setting for phosphogenesis. *Chemical Geology* 395, 88–107.

II Lepland, A., **Joosu, L.**, Kirsimäe, K., Prave, A.R., Romashkin, A.E., Crne, A.E., Martin, A.P., Fallick, A.E., Somelar, P., Upraus, K., Mand, K., Roberts, N.M.W., van Zuilen, M.A., Wirth, R., Schreiber, A. (2014) Potential influence of sulphur bacteria on Palaeoproterozoic phosphogenesis. *Nature Geoscience* 7, 20–24.

III Lepland, A., Melezhik, V.A., Papineau, D., Romashkin, A.E., **Joosu, L.** (2013). The earliest phosphorites: radical change in the phosphorus cycle during the Palaeoproterozoic. In: Melezhik, V.A., Prave, A.R., Hanski, E.J., Fallick, A.E.; Lepland, A., Kump, L. (Eds.). *Reading the Archive of Earth's Oxygenation*. Volume 3: *Global Events and the Fennoscandian Arctic Russia – Drilling Early Earth Project*. Springer, pp. 1275–1296.

IV **Joosu, L**., Lepland, A., Kreitsmann, T., Üpraus, K., Roberts, N.M.W., Paiste, P., Martin, A.P., Kirsimäe, K. (2015) Petrography and the REE-composition of apatite in the Paleoproterozoic Pilgujärvi Sedimentary Formation, Pechenga Greenstone Belt, Russia. Manuscript submitted to *Geochimica et Cosmochimica Acta*.

Author's contribution:

Paper I: The author was primarily responsible for planning original research, data collection, participated in REE analysis and interpretation of analytical results, synthesis of mineralogical-geochemical analytical data and writing of the manuscript.

Paper II: The author was responsible for planning research, data collection and scanning electron microscope analysis and interpretation of analytical results, and contributed to the writing of the manuscript.

Paper III: The author was responsible for petrographical and mineralogical analysis and interpretation of analytical results.

Paper IV: The author was primarily responsible for planning original research, data collection, participated in REE analysis and interpretation of analytical results, synthesis of mineralogical-geochemical analytical data and writing of the manuscript.

1. INTRODUCTION

Phosphorus is an essential and non-substitutable element for life being a key component in many important macro-molecules (DNA, RNA, ATP etc.). It is therefore one of the most important nutrients limiting primary productivity (Vitousek et al. 2010; Pufahl and Hiatt 2012). There is an ever-growing global demand for phosphorous as a fertilizer while the known phosphate rock (phosphorite) reserves are depleting (Obersteiner et al. 2013).

In the natural P-cycle most of the phosphorous is derived from continental weathering and carried fluvially into oceans (Filippelli 2008). However, the concentration of dissolved phosphorus in seawater is very low (ca. 40–60 µmol/g, Filippelli 2002) because the reactive (dissolved) phosphorous is efficiently used up by primary producers in the photic zone of the water column (Fröelich et al. 1982; Ammerman et al. 2003). Phosphorus is removed from seawater by burial of organic matter as well as by scavenging onto iron-manganese oxide particles (Filippelli 2008). A major sink of phosphorous and the formation of P-rich deposits – phosphorites – occurs at the continental margins and/or in coastal areas influenced by upwelling ocean currents. In these locations P-rich deep ocean water stimulates primary production leading to deposition of organic-rich sediments with organically bind polyphosphate; modern examples of this are the Namibian and the Peruvian shelves (Föllmi 1996).

The Ca-phosphate mineral apatite is the most common authigenic stable solid phosphate phase in phosphorite sediments, but the link between polyphosphate release from organic matter and apatite precipitation within sediments is poorly understood (Koutsoukos and Valsami-Jones 2004). Precipitation of apatite within sediments requires: (i) a source of phosphorous (e.g. degradation of organic matter or desorption from iron-manganese oxide particles), and (ii) a concentration mechanism to achieve supersaturation with respect to the phosphate that is required for precipitation of a solid phase.

The main sites of modern phosphogenesis with elevated interstitial dissolved P and availability of nucleation templates favoring the apatite precipitation are the shallow levels of the sediment column, close to the sediment water interface within the sulfidic to suboxic/oxic diagenetic zone (Jarvis et al. 1994). Diagenetic desorption of scavenged phosphate from Mn/Fe-oxyhydroxides (Berner 1973) and the release of phosphate from bacterially decomposed organic matter (Krajewski et al. 1994) have traditionally been considered as the main processes building up the interstitial phosphate concentration needed for apatite precipitation. More recent studies of organic-rich sediments on modern continental margins (Schulz et al. 1999; Schulz and Schulz 2005; Arning et al. 2008; 2009a,b) and laboratory experiments (Goldhammer et al. 2010; Brock and Schulz-Vogt 2011) have revealed the utmost significance of sulfur-oxidizing bacteria mediating redox-dependent phosphorous-cycling by creating sinks for marine phosphorous and eventually phosphorite formation. Several genera of sulphur-oxidising bacteria that are capable of storing intracellular polyphosphate reserves (e.g. *Beggiatoa, Thiomargarita*) exist in the shallow sediments

with periodically fluctuating (sub)oxic-sulphidic conditions. Under anoxic conditions, sulfur-bacteria hydrolyse the polyphosphate stored intracellularly under oxic conditions, and release phosphate (Figure 1; Brock and Schulz-Vogt 2011; Schulz and Schulz 2005). As a result, the bacterial phosphate "pumping" leads to supersaturation of the pore water with respect to apatite and which rapidly precipitates, probably via an amorphous metastable Ca-phosphate precursor (Arning et al. 2009b; Goldhammer et al. 2010).

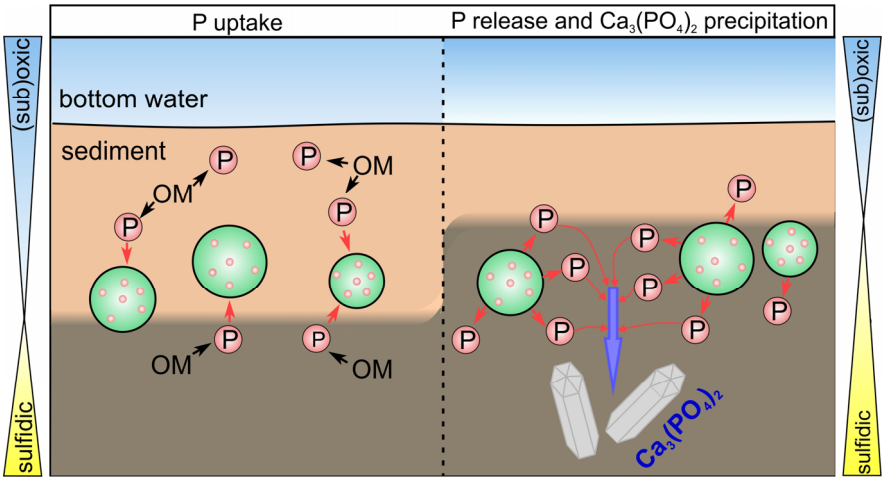

Figure 1. Sulfur bacteria mediated phosphogenesis in coastal marine sediments (modified from Brock and Schulz-Vogt 2011). Under oxic conditions sulfur-oxidizing bacteria store polyphosphate. Under anoxic conditions, sulfur-bacteria hydrolyse the polyphosphate and release phosphate that leads to calcium phosphate precipitation.

Formation of phosphorite deposits is mainly a Phanerozoic phenomenon, but the first significant P-rich deposits seem to appear contemporaneously worldwide in the Paleoproterozoic rock record in around 2 Ga (Papineau 2010). Their appearance has been linked to the oxidation of the atmosphere and establishment of the aerobic, modern-type Earth at about 2.3 Ga, known as the Great Oxygenation Event (GOE) (Bekker et al. 2004). This triggered extensive oxidative weathering of continental landmasses, which in turn led to enhanced discharges of reactive phosphorous into the ocean and the blooming of primary producers (Melezhik et al. 2005; Papineau 2010; Pufahl et al. 2010; Bekker and Holland 2012). However, the increased inflow of continentally derived P did not cause phosphorite formation immediately following the GOE. Furthermore, it took ca 300–400 Ma from the GOE to the beginning of Paleoproterozoic phosphogenisis. Environmental settings of the modern phosphogenesis highlight the link between marine phosphorous and sulfur cycling in the shallow levels of the sediment column within the sulfidic to (sub)oxic diagenetic zone possibly suggesting that a build up of a marine sulfate reservoir and sulfur cyc-

ling within sediments was needed to initiate phosphogenesis. As seawater sulfate concentrations increased in response to the oxygenation of the Earth (e.g. Reuschel et al. 2012) the specific environmental conditions suitable for both sulfur reducing and oxidizing microorganisms were established at the sediment-water interface and in shallow subsurface sediments for the first time in Earth history, possibly triggering the onset of microbially mediated phosphogenesis.

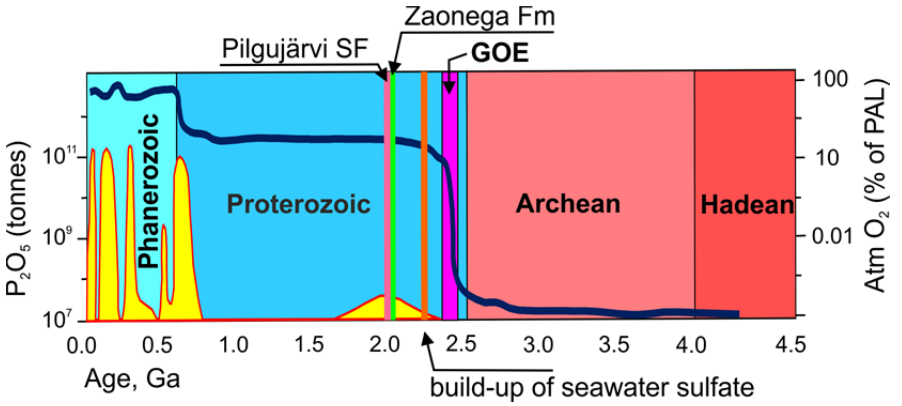

Figure 2. Temporal distribution of P-rich rocks (yellow; after Pufahl and Hiatt 2012), evolution of atmospheric oxygen (blue line; after Kump 2008) and selected Paleoproterozoic global events. GOE – Great Oxidation Event marks the rise of O_2 between 2.45–2.32 Ga after Bekker et al. (2004). Timing of seawater sulfate build-up at 2.1 Ga is after Reuschel (2012). Depositional ages of Zaonega Fm (1.97 Ga) and Pilgujärvi SF (1.92 Ga) after Martin et al. (2015).

However, the specific mechanisms that led to the formation of P-rich sediments and precipitation of Ca-phosphate minerals in the Paleoproterozoic are still unclear (e.g. Papineau 2010). Apart from specific mechanisms – e.g. Fe/Mn redox pumping, bacterial sulfate reduction and/or sulfur-bacteria pumping (Krajewski et al. 1994; Nelson et al. 2010; Schulz and Schulz 2005) – phosphate concentration and precipitation in the Paleoproterozoic would have required the establishment of suboxic or oxic conditions in the seawater. Most importantly, development of fluctuating redox conditions in shallow sediment depths below the sediment – water interface is critical for concentrating interstitial phosphate.

Environmental conditions of phosphogenesis can be assessed by rare earth element (REE) analysis of sedimentary phosphate occurring primarily in the form of the Ca-phosphate mineral apatite. During precipitation, the REEs are incorporated into the apatite structure by substitution for Ca. The REE uptake by early digenetic apatite is considered to be quantitative, and consequently the REE composition of apatite reflects the REE signatures of sediment pore water and the overlying water column (Jarvis et al. 1994). The REE patterns and, in particular, relative enrichment or depletion of redox sensitive Eu and Ce, can be

used for deciphering the environmental conditions of phosphogenesis. Negative Ce anomalies indicate an oxygenated water column, in which Ce^{3+} is oxidized to Ce^{4+} and is removed by Fe-Mn oxyhydroxide precipitates (McArthur and Walsh 1984). Positive Ce anomalies are the result of reductive dissolution of Fe-Mn oxyhydroxide in anoxic/euxinic waters (Mazumdar et al. 1999). Positive Eu anomalies can be generated in strongly reducing environments where Eu^{3+} is reduced to mobile Eu^{2+} (Bau 1991). These are often associated with hydrothermal fluids and when recorded in apatite indicate precipitation under the influence of hydrothermal fluids (Garnit et al. 2012; Shields and Stille 2001).

One of the oldest occurrences of P-rich sedimentary rocks in Earth's history is found in association with ca. 2 Ga old sediments rich in organic matter in the Zaonega Formation (Zaonega Fm), Onega basin Karelia, Russia; and in nearly coeval P-rich shales and gritstones-sandstones of the Pilgujärvi Sedimentary Formation (Pilgujärvi SF) in Pechenga Greenstone Belt (hereafter Pechenga basin), Kola peninsula, Russia (Lepland et al. 2013 – Paper III). These sedimentary rocks accumulated in magmatically active basins experiencing widespread hydrothermal venting (Melezhik and Hanski 2013; Črne et al. 2013).

This thesis studies the petrography and the REE abundances of sedimentary apatite in the Zaonega Fm and Pilgujärvi SF. The main aims of the thesis are:

1) to document the petrographical and compositional characteristics of apatite in Zaonega Fm and in Pilgujärvi SF;
2) to assess the preservation of sedimentary/early digenetic REE signatures in apatite reflecting ancient sea water;
3) to interpret and compare the environmental conditions with an emphasis on the redox state during formation of Zaonega and Pilgujärvi P-rich sediments.

The thesis puts forward a central hypothesis that if the oxygen and sulfate concentrations of the water masses increased as a consequence of the Great Oxygenation Event, then (sub)oxic-sulfidic redoxclines were established at shallow sediment depth facilitating Ca-phosphate precipitation through either Fe/Mn redox pumping, bacterial sulfate reduction and/or sulfur-bacteria pumping mechanisms. Establishment of such conditions is possibly recorded in the REE composition of the sedimentary apatite.

2. GEOLOGICAL SETTING

Material studied in this thesis was sampled from two Paleoproterozoic basins in northwestern Russia – Onega Basin, Karelia and Pechenga Greenstone Belt (hereafter Pechenga Basin) in the Kola Peninsula (Figure 3).

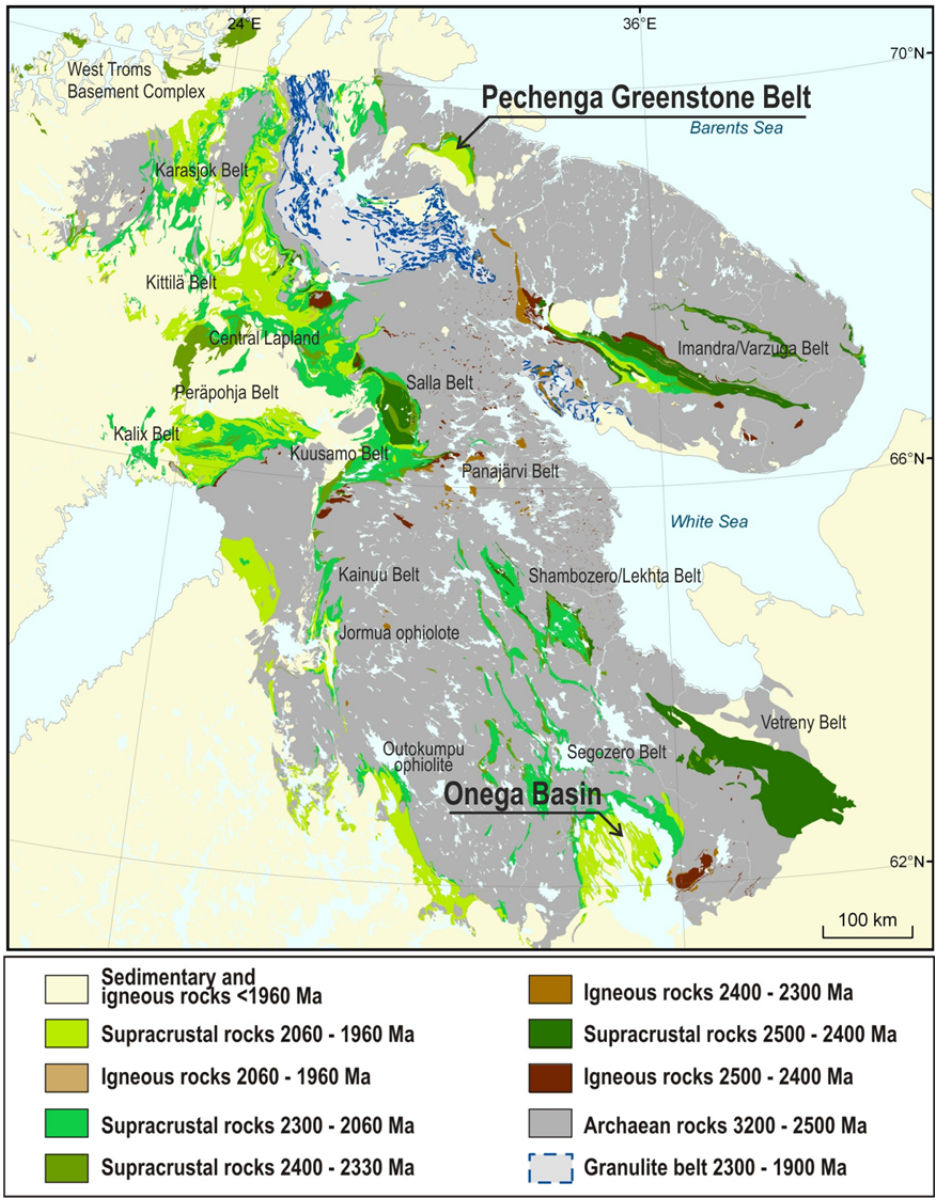

Figure 3. Location of Onega basin and Pechenga Greenstone Belt in the Fennoscandian Shield (modified from Melezhik et al. 2013 and Koistinen et al. 2001).

2.1. Zaonega Formation

The Onega Basin is a part of the Paleoproterozoic supracrustal succession in central Karelia, north-western Russia, forming a large NW–SE-trending synform and outcropping around the northern shore of Lake Onega (Figure 4). The succession of the Onega Basin consists upwards of the Glubokozero and Kumsa formations (mafic magmatic and sedimentary rocks), Paljozero and Jangozero formations (conglomerates, gritstones, quartzites), Medvezhegorsk Formation (basalts), Tulomozero Formation (stromatolitic dolostones, evaporitic dissolution breccias, quartz sandstones, siltstones), Zaonega Formation (basalts, sandstone, mudstone, dolostone, limestone, chert, maffic tuffs, all of which are intruded by gabbroic sills), and the Suisari Formation (basalts, tuffs), overlain by younger, mostly siliciclastic sedimentary rocks (see Melezhik and Hanski 2013 for an overview). The succession was deformed and underwent regional, maximum greenschist facies metamorphism during the Svecofennian Orogeny at 1.89-1.79 Ga (Melezhik and Hanski 2013).

During Paleoproterozoic times, this area was a basin along the rifted margin of the Karelian craton that faced the Svecofennian Ocean (Melezhik et al. 1999). The maximum age of the Zaonega Formation is robustly constrained by the underlying Burakovka Pluton dated at 2449 ± 1 Ma (Amelin et al. 1995). The minimum age may be constrained by a 1969 ± 18 Ma Re-Os isochron age from the overlying Suisari Formation (Puchtel et al. 1999). A variety of dating techniques on units in the Onega Basin suggest the Zaonega Fm is younger than 2060 Ma (Hannah et al. 2008; Hannah et al. 2010; Ovchinnikova et al. 2007; Puchtel et al. 1998). Chemostratigraphic correlation supports previous dates and constrains the age of the Zaonega Formation younger than 2058.6 ± 0.8 Ma (Martin et al. 2013; Melezhik et al. 2007) as the Lomagundi-Jatuli carbonate carbon isotope excursion is recorded in underlying Tulomozero Formation. Recently, Martin et al. (2015), limited the age of deposition of the zaonega sediments close to the previously proposed youngest age, between 1975.3 ± 2.8 and 1967.6 ± 3.5 Ma.

The Zaonega Fm is composed of magmatic, siliciclastic and carbonate rocks with several organic carbon-rich intervals. Interbedded greywacke and mudstones represent turbidity-current deposits whereas mudstone packages represent background hemipelagic sedimentation (Črne et al. 2013). Sedimentary rocks are interlayered and intersected by numerous syn-depositional tuffs, lavas and sills, and magmatic rocks constitute more than half of the Zaonega Fm succession suggesting a magmatically active depositional environment, possibly an intraplate rift setting (Črne et al. 2013).

Peperite contacts of some gabbros indicate the intrusion of magmatic bodies into wet, unconsolidated sediments. These intrusions triggered hydrothermal circulation and initiated hydrocarbon formation and migration (Črne et al. 2013). It has been argued that the Zaonega Fm represents one of the earliest significant petroleum deposits on the planet (Buseck et al. 1997; Črne et al. 2013, Melezhik et al. 1999). Hydrocarbon seepage potentially provided habitats for

methane metabolizing microbial communities and resulted in the negative $\delta^{13}C$ shift in organic carbon matter observed in the upper part of the Zaonega Fm (Qu et al. 2012). Whole rock redox indicators such as Mo and U concentrations and a degree of pyritization are stratigraphically variable, suggesting alternation of redox conditions during the accumulation of Zaonega sediments (Asael et al. 2013, Partin et al. 2013, Scott et al. 2008). Phosphorus concentrations in the lower and middle part of the Zaonega Fm are generally low (P_2O_5 less than 0.5 %). P-rich intervals (P_2O_5 > 1 %) have been reported from organic-rich dolostones and mudstones in the upper part of the formation (Črne et al. 2013; Lepland et al. 2013 – PAPER III).

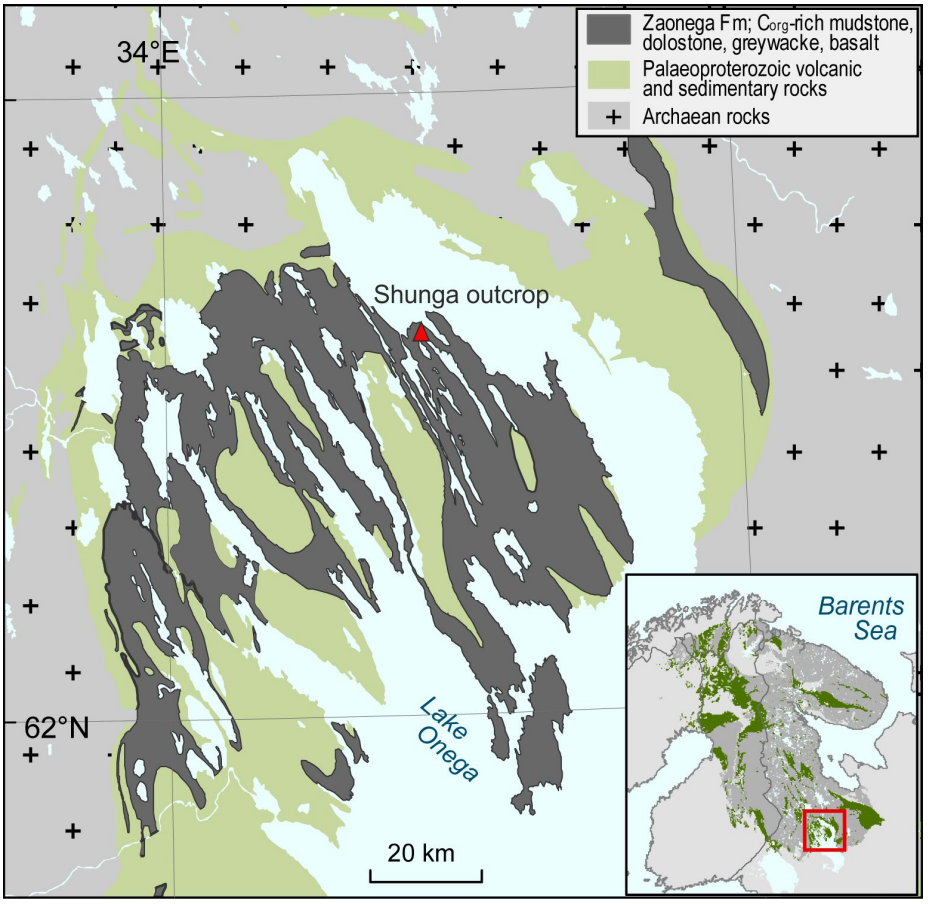

Figure 4. Simplified geological map of the Paleoproterozoic Onega Basin (modified after Koistinen et al. 2001) with the location of the sampled Shunga outcrop (red triangle) in the Zaonega Fm.

2.2. Pilgujärvi Sedimentary Formation

The Pechenga basin belongs to the ca. 800 km long Paleoproterozoic supracrustal Transfennoscandian Greenstone Belt (Melezhik and Sturt 1994) in the northwestern part of the Kola Peninsula, Russia (Figure 5). It hosts large reserves of Ni-Cu-sulfide ore and its geology has been comprehensively reviewed recently in Melezhik and Hanski (2013). The North Pechenga Group studied in this thesis is composed of eight formations (Figure 5) including the Pilgujärvi SF and Pilgujärvi Volcanic Formations at the top of the group.

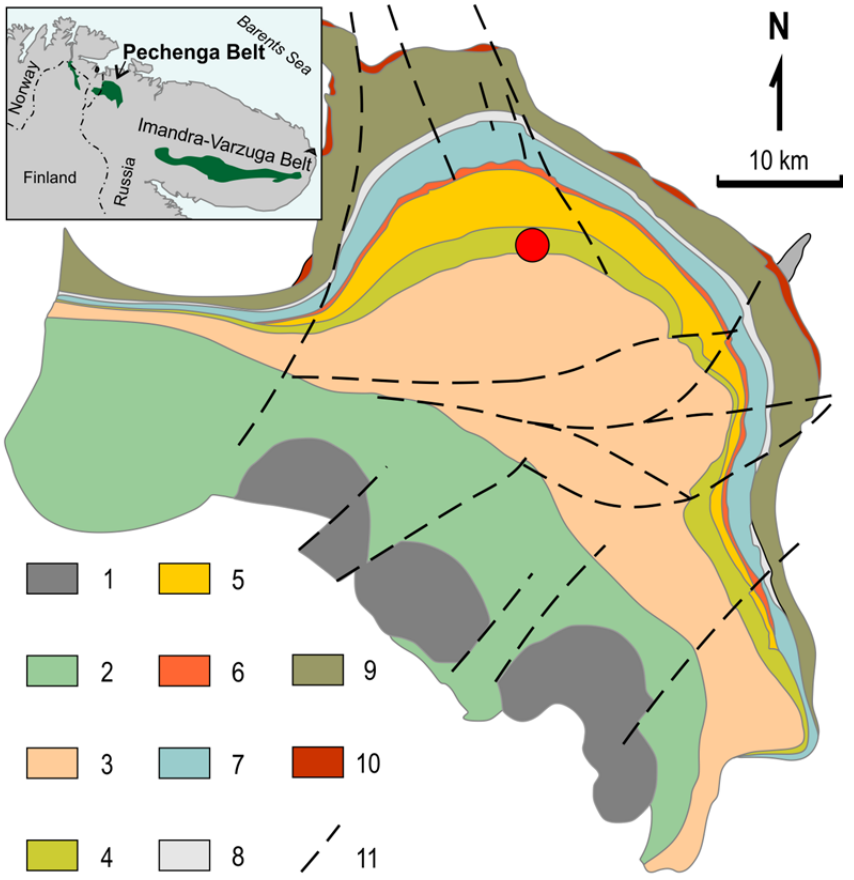

Figure 5. Simplified geological map of Pechenga Greenstone Belt (modified after Hanski et al. 2014). Legend: 1 – granodiorite intrusives, 2 – South Pechenga Group (undifferentiated), North Pechenga Group: 3 – Pilgujärvi Volcanic Formation, 4 – Pilgujärvi Sedimentary Formation, 5 – Kolosjoki Volcanic Formation, 6 – Kolosjoki Sedimentary Formation, 7 – Kuetsjärvi Volcanic Formation, 8 – Kuetsjärvi Sedimentary Formation, 9 – Amalahti Formation, 10 – Neverskukk Formation, 11 – faults. Red dot shows the location of the sampling site.

The Pilgujärvi SF is the thickest sedimentary succession of the Pechenga basin reaching in total ca. 1000 m in thickness. The Pilgujärvi SF includes numerous mafic-ultramafic sills and minor lavas (ca. 500 m in total thickness). The Pechenga Ni-Cu-sulfide deposits occur within the contact zones of sills and sedimentary host rocks (Melezhik and Hanski 2013). The Pilgujärvi SF sedimentary sequences are dominated by rhythmically interbedded C_{org}- and sulfide-rich turbiditic greywacke-shales and tuffs deposited in a deep-water, shelf environment as turbiditic sequences (Ahmedov and Krupenik 1990; Melezhik and Stuart 1998).

The maximum age of the Pilgujärvi SF is constrained by zircon age of 1922.6 ± 1.1 Ma of the Kolosjoki Volcanic Formation, stratigraphically beneath the Pilgujärvi SF (Martin et al. 2015) and the underlying sediments of the Kolosjoki Volcanic Formation that yield detrital zircon grains dated at 1916 ± 1 Ma (Gärtner et al. 2011). Sampled from near the base of the Pilgujärvi SF, detrital zircon provides a maximum age to deposition at 1922.8 ± 1.6 Ma (Martin et al. 2015) though various single isochron methods on mafic intrusions and organic-rich shale provide a range of older (maximum) ages between 2231 and 1924 Ma (Hannah et al. 2006; Hanski et al. 1990; Walker et al. 1997). Nevertheless, zircon grains in a tuff in the Pilgujärvi Volcanic Formation, immediately overlying the Pilgujärvi SF, have yielded a 1919.2 ± 1.3 Ma age (Martin et al. 2015). Thus deposition of the Pilgujärvi SF is constrained to between 1922.8 ± 1.6 Ma and 1919.2 ± 1.3 Ma (Martin et al. 2015; Joosu et al. 2015b – PAPER IV).

Phosphorus-rich intervals in Pilgujärvi SF occur as lenses and a series of gritstone and coarse-grained sandstone beds within a 50–250 m-thick succession of rhythmically bedded greywacke- sandstone-siltstone-shale in the central part of the Pilgujärvi SF sequence (Bekasova and Dudkin 1981). Rounded to angular phosphatic particles (0.2–5 mm in size) typically occur in the most coarse grained, lower part of the sequence, which is composed of clasts of quartz [40–54 volume (vol) %], feldspar (7–10 vol%), quartzite-silicified shale (7–30 vol%) and lithic clasts of mafic lava (3–30 vol%) (Bekasova and Dudkin 1981). The phosphatic particles form less than 5 vol% of the gritstone and are composed of fluor-carbonate apatite (francolite) with a varying admixture of mostly silt-size quartz, feldspar and mudstone fragments and organic matter (3-5 wt%, Bekasova and Dudkin 1981). Locally, the P-rich gritstones show high abundances of pyrite and pyrrhotite clasts (> 50 vol% in places), with sizes from < 1 mm to 20 mm, including outsized, angular or rounded and softly-deformed fragments of siltstone and mudstone, as well as softly-deformed fragments of bedded and laminated siltstone-mudstone (Lepland et al. 2013 – PAPER III; Joosu et al. 2015b – PAPER IV).

Pilgujärvi SF P-rich coarse grained beds are interpreted as proximal facies of a submarine fan delta and/or possibly submarine slope-slide facies deposits at the seaward slope of a marine shelf (Akhmedov and Krupenik 1990; Melezhik and Stuart 1998) whereas the relatively large phosphatic clast of the P-rich

sediment along with other abundant locally derived clasts (mudstone, pyrite etc.) indicates a short transport distance (Lepland et al. 2013 – PAPER III).

Rozanov et al. (2007) and Rosanov and Astafieva (2008) have described abundant and diverse remains of putative fossilized filamentous, coccoid, oval and rod-shaped microorganisms in the phosphatic particles from Pilgujärvi SF. Morphology of the described microbial structures resemble cyanobacteria reported from modern alkaline or saline environments, suggesting possibly cyanobacterial mat structures as sites for phosphogenesis in Pilgujärvi SF (Rozanov and Astafieva 2008). Similar to Onega Basin the Pechenga basin encompassing the Pilgujärvi SF underwent the regional, maximum greenschist facies metamorphism during the Svecofennian Orogeny at 1.89-1.79 Ga (Melezhik and Hanski 2013).

3. MATERIALS AND METHODS

The P-rich samples of Zaonega Fm studied, were collected from the outcrop section near Shunga village (Figure 4) where the rocks of the upper part of the Zaonega Fm are exposed in a ca. 13 m high cliff. The lower part of the outcrop consists of a 5 m thick succession of black, organic-rich mudstone that contains two dolostone beds and a ca. 15 cm thick seam of lustrous pyrobitumen (petrified petroleum). Black mudstone is in places coated by a thin yellowish layer of secondary jarosite due to surface weathering of pyrite. The upper part of the outcrop is composed of alternating chert and dolostone. Some contacts between the chert and the dolostone are transitional with indications of chert replacing dolostone. Twenty-three samples were collected from the phosphorus rich interval in the middle of the Shunga outcrop comprising of two mudstone units and a dolostone for geochemical and mineralogical characterization, of these eight polished slabs of samples with elevated P_2O_5 content were used for petrographic characterization and laser ablation inductively coupled plasma mass spectrometry (LA-ICP-MS) studies (Joosu et al. 2015a – PAPER I).

Pilgujärvi SF P-rich rocks do not crop out but have been previously documented in drill cores (Bekasova and Dudkin 1981; Melezhik and Stuart 1998; Lepland et al. 2013 – PAPER III). Locally they are displaced into spoil tips during open-pit mining of Cu-Ni sulfide ores. One such spoil tip (69 24’35’’N 30 38’15’’E) ca. 7 km WSW of Zapolyarny (Figure 5) comprises numerous meter scale, fresh blocks of rhythmically bedded greywacke-sandstone-siltsone with gritstone-sandstone intervals containing abundant phosphatic particles. Lithological similarities between P-rich gritstone-sandstone horizons in previously studied drill cores and within these blocks suggests that they were likely to have been derived from the middle part of the Pilgujärvi SF, although the exact stratigraphic position remains unknown. Samples used in this study were collected from five different blocks (Joosu et al. 2015b – PAPER IV).

The mineralogical composition of whole rock samples from both formations was studied by means of X-ray diffractometry (XRD). Samples were pulverized in a planetary mill and unoriented preparations were made. XRD patterns were scanned on Bruker D8 Advance diffractometer using Cu*K*α radiation and LynxEye positive sensitive detector in 2–70° 2Theta range. The quantitative mineralogical composition of the samples was interpreted and modeled by using the Rietveld algorithm-based program Siroquant-3 (Taylor 1991).

Major and trace element compositions of Zaonega Fm rocks were measured at ACME Analytical Laboratories, Canada using inductively coupled plasma optical emission spectrometry. Homogenized and pre-ignited (1000 °C) 0.2 g samples were fused in a lithium metaborate tetraborate mixture and digested in nitric acid. The major element composition of Pilgujärgi SF samples was analyzed using an X-ray fluorescence (XRF) Rigaku Primus II spectrometer in pressed powdered samples at the Department of Geology, University of Tartu, Estonia.

Polished slabs and petrographic thin sections were prepared and studied with both a petrographic optical microscope and a scanning electron microscope (SEM) using a variable pressure Zeiss EVO MA15 SEM equipped with an Oxford X-MAX energy dispersive detector system and AZTEC software for element analysis at the Department of Geology, University of Tartu, Estonia; and a LEO 1450VP SEM equipped energy dispersive detector system from Oxford Instruments and Inca software for elemental analysis at the Norwegian Geological Survey, Norway.

REEs in apatite were measured at the Natural Environment Research Council Isotope Geosciences Laboratory (NIGL), U.K. and Department of Geology, University of Tartu, Estonia by laser ablation inductively coupled plasma mass spectrometry (LA-ICP-MS). Measurements at NIGL were performed using a Nu Instruments AttoM single-collector ICP-MS in linkscan mode, coupled to a New Wave Research UP193ss with a fast-washout two-volume large-format cell. Typical ablation parameters at NIGL included a 35 µm spot, at 5Hz and ~2.5 j/cm^2 fluence, with a 40 second dwell time. At the University of Tartu an Agilent 8800 quadrupole ICP-MS coupled to a Cetac 213 nm HelEx fast-washout two-volume large-format cell using 40 µm spot, at 5 Hz and ~2.5 j/cm^2 fluence, with a 40 second dwell time was used. Helium was used as a carrier gas in both instruments and was mixed with argon from a desolvating nebuliser. The following masses were measured: ^{139}La, ^{140}Ce, ^{141}Pr, ^{146}Nd, ^{149}Sm, ^{153}Eu, ^{157}Gd, ^{163}Dy, ^{165}Ho, ^{167}Er, ^{172}Yb, ^{175}Lu, and were normalized to ^{44}Ca assuming 39.7% Ca in the apatite mineral. Tb and Tm were not analyzed. Concentrations were normalized to NIST612 values from Jochum et al. (2011), which was analyzed four times after every ten samples. The reproducibility of NIST612 within each analytical session was better than 10 % for each mass measured with both instruments. During LA-ICP-MS analysis, oxides from Ba interfere with Eu, and LREE oxides interfere with the HREE (Kent and Ungerer 2005). The rate of Ba- and LREE-oxide formation is similar to or less than that of Th-oxide, as measured in separate analytical session, and oxides monitored during analysis were <0.3 % for UO/U and <0.6 % ThO/Th.

Measured REE abundances were normalized against Post Archaean Average Shale (PAAS, Taylor and McLennan 1985). The PAAS normalized abundances are marked with subscript "N" after the element symbol. Anomalies are presented as the ratio of measured and calculated values of any given element. "*" denotes the theoretical value calculated using neighboring elements. Lanthanum and Ce anomalies were calculated geometrically by extrapolating back from Pr and Nd abundances assuming that the ratio between neighboring elements remains constant and using the equations: $La/La^* = La_N/[Pr_N*(Pr_N/Nd_N)^2]$ and $Ce/Ce^* = Ce_N/[Pr_N*(Pr_N/Nd_N)]$ (Mclennan 1989). This approach was selected to avoid La anomaly interference on Ce anomaly assessment. Praseodymium and Nd were selected as references because there is no known mechanism for Pr and Nd fractionation (Bau and Dulski 1996). The Eu anomaly was calculated as the half sum of neighbouring elements – $Eu/Eu^* = Eu_N/((Sm_N+Gd_N)/2)$, Y anomaly was calculated as $Y/Y^* = Y_N/((Dy_N+Ho_N)/2)$ (Byrne and Sholkovitz 1996).

4. RESULTS

4.1. Ca-phosphate in Zaonega Formation

4.1.1. Distribution and petrography of phosphate in Zaonega Fm

The highest P content in the Shunga outcrop section of the Zaonega Fm is found in a ca. 15 cm thick interval within the lower mudstone unit just below the dolostone contact (Figure 6), where P_2O_5 abundance reaches 16.3 wt. % (Lepland et al. 2014 – PAPER II; Joosu et al. 2015a – PAPER I). The principal carrier phase of phosphorous in samples studied is apatite, but trace amounts of monazite and xenotime have also been identified. Additional main phases in the finely laminated mudstone include organic matter and phlogopite, possibly derived from Mg(Fe)-rich clay (Lepland et al. 2014 – PAPER II) and minor pyrite that forms small euhedral crystals or has framboidal habit (Joosu et al. 2015a – PAPER I).

The SEM backscattered electron (BSE) imaging shows that apatite occurs as impure laminae, lenses and round-oval nodules and is typically intergrown with organic matter. Apatite lenses and nodules may occur individually in the mudstone matrix or form clusters that can be arranged into layers, with a thickness as much as several mm (Figure 7). Individual lenses and nodules within such clusters are separated from each other by thin lamina rich in organic matter. Apatite nodules are typically elongated parallel to bedding and reveal some deformation and flattening. Apatite laminae and lenses show occasional deflections similar to mudstone hostrock, indicating their soft nature during compaction. These features are consistent with the proposed early diagenetic, prelithification origin of apatite structures (Lepland et al. 2014 – PAPER II).

Within laminae, lenses and nodules, the apatite occurs predominantly as cylindrical aggregates/particles imprinted into the matrix of organic matter and the phlogopite (Figure 5). Apatite cylinders have diameters of ca. 0.5-4 μm and lengths of ca. 1–8 μm (Lepland et al. 2014 – PAPER II). The cylinders have been variably recrystallized with the best preserved end-member consisting of nanometer scale crystallites intergrown with finely dispersed organic matter and the most altered end-member forming a cylindrical single crystal of apatite. In between those two end-members there are progressive recrystallizations with apatite crystallites growing from the outer rim of the cylinder towards the center until a single crystal is formed, during which, organic matter inclusions are excluded. Apatite cylinders may be sparsely distributed in the matrix of organic matter or closely packed so that individual cylinders are indistinguishable (Figure 7D).

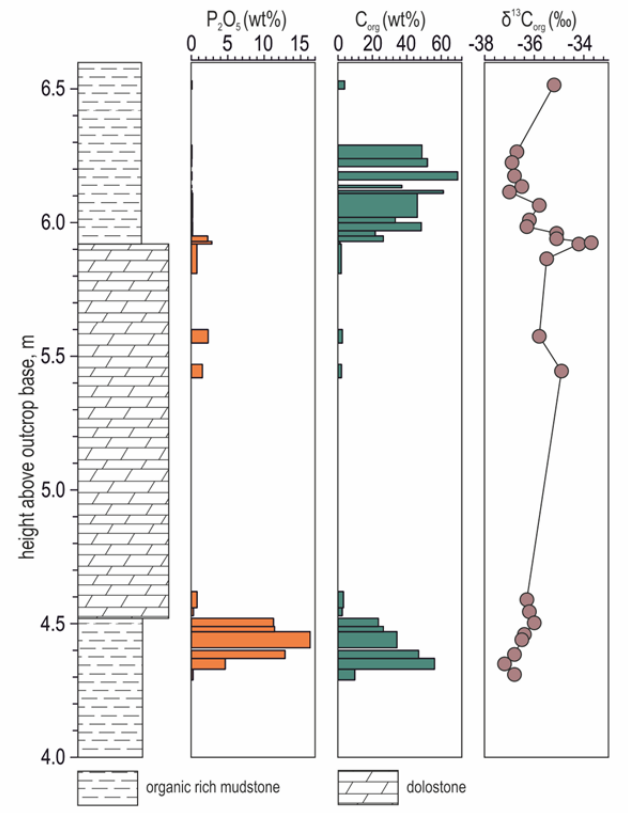

Figure 6. Geochemical profiles through the P-rich interval of the Zaonega Fm exposed in a ca. 13 m thick outcrop at Shunga village. (Lepland et al. 2014 – PAPER II).

Secondary, post-lithification veins cross cut the mudstone units and apatite structures (layers lenses, nodules). The composition of these veins is variable but controlled by the host lithology (Figure 7A). In mudstones, the veins are predominantly composed of phlogopite whereas within apatite structures they consist of larger (tens of micrometers in size), closely packed, anhedral, impurity-free apatite crystals. Formation of such anhedral apatite in cross–cutting veins is possibly related to fluid interaction with the host apatite structure causing recrystallization of earlier generation impurity-rich fine-crystalline apatite. The veining-related recrystallization did not apparently result in significant phosphate mobilization since the anhedral crystallites of vein apatite are predominantly confined within veins cross-cutting apatite structures (Joosu et al. 2015a – PAPER I).

Samples from the dolostone unit in the Shunga outcrop contain up to 2.3 wt.% of P_2O_5. Apatite in dolostone occurs at infrequent intervals where it forms black discontinuous layers up to 1 cm thick (Figure 7E). Apatite is found filling the pore space and in a few cases replacing dolomite or calcite crystals (Figure 7A).

In some areas with a high organic carbon content, the embedded apatite particles show finely dispersed inclusions of organic matter indicating limited recrystallization. Overall, apatite within dolostone seems to be more strongly affected by recrystallization than apatite in mudstone units.

The upper mudstone unit above the dolostone has a lower P_2O_5 concentration (< 3 wt.%) than the lower mudstone unit. However, the apatite in the upper mudstone unit has similar petrographic characteristics to the lower mudstone unit (Joosu et al. 2015a – PAPER I).

Based on petrographic characterization, apatite in P-rich intervals of the Zaonega Fm in Shunga outcrop can be divided into four types (Joosu et al. 2015a – PAPER I):

1) Diagenetic apatite (DiaAp) occurring as cylinders or aggregates consisting of nanocrystalline particles or apatite single crystallites imprinted into organic matter rich matrix. In some cases particles are tightly packed and their margins/contacts are not observed.
2) *In situ* partially recrystallized apatite (hereafter referred to as partially recrystallized apatite – PartRecAp) occurring as DiaAp that may have been affected by partial recrystallization. The main criterion used to evaluate recrystallization was the percentage of finely dispersed organic matter inclusions. Apatite belonging to this group has up to 80% surface area free of organic matter. The distinction between DiaAp and PartRecAp is not sharp and some LA-ICPMS spots assigned in this group may represent DiaAp, but by including such transitional spots within PartRecAp assures that the type defined as DiaAp is least affected by recrystallization.
3) *In situ* recrystallized apatite (RecAp) revealing a clear recrystallization pattern. The area occupied by finely dispersed organic matter inclusions is below 20 %, although this apatite may contain some bigger organic matter inclusions. Recrystallization occurs without obvious influence of filtrating fluids.
4) Vein apatite (VeinAp) formed by infiltrating fluids. Apatite crystals are up to tens of μm in size with no or minor organic matter inclusions. Individual apatite cylinders are not present.

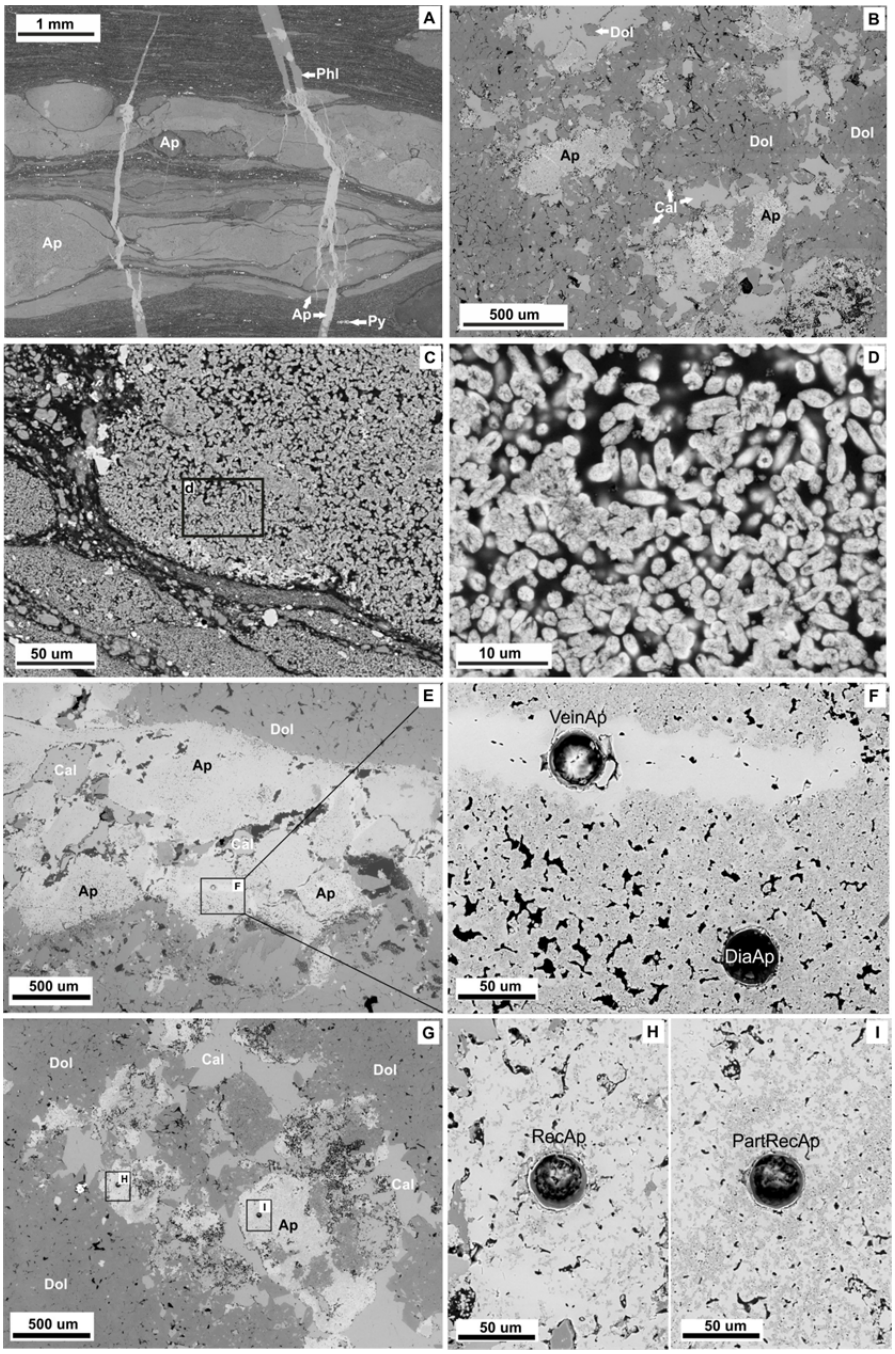

Figure 7. SEM-BSE images illustrating apatite petrography in the Shunga outcrop, Zaonega Fm. (A) lower mudstone unit exhibiting apatite-rich laminae, lenses and nodules in organic matter rich mudstone matrix. (B) Dolostone hostrock with the inclusion of variable quantities of organic matter. (C-D) Images illustrating the occurrence of phosphatic nodules (C) and apatite cylinders within it (D). (E-I) Apatite-rich

lamina in dolostone. (F) Diagenetic apatite (DiaAp) and vein apatite (VeinAp). (H) Recrystallized apatite with minor organic matter inclusions. (I) Partly recrystallized apatite with abundant organic matter inclusions. Ap – apatite, Phl – phlogopite, Py – pyrite, Dol – dolomite, Cal – calcite.

4.1.2. Rare Earth Element composition of apatite in Zaonega Fm

The REE characteristics of apatite in samples from the lower mudstone unit Zonega Fm are broadly similar to each other, with minor, but consistent differences between individual petrographic types (Joosu et al. 2015a – PAPER I). PAAS normalized DiaAp and PartRecAp REE patterns are similar to each other with flat mid (M)-REEs (Gd_N to Er_N) and depleted light (L)-REEs (La_N/Sm_N) and heavy (H)-REEs ($Er_N/Lu_{N)}$ (Figure 8). La_N/Sm_N is = 0.6 and 0.6, and average Er_N/Lu_N is 1.8 and 1.7 in DiaAp and PartRecAp, respectively. RecAp and VeinAp REE patterns are alike but relative to DiaAp and PartRecAp show more pronounced depletion of LREEs and HREEs, as MREEs decrease slightly towards Er (respectively La_N/Sm_N is = 0.3 and 0.3, Gd_N/Er_N is = 1.4 and 1.3 and Er_N/Lu_N is = 3.2 and 3.1). There is a small but uniform negative Ce anomaly with an average value of 0.8 in all apatite types. Europium exhibits consistently positive anomalies with average Eu/Eu* values of 2.0 in DiaAp and RecAp and slightly higher (2.1) in PartRecAp and VeinAp. Positive La anomalies are highest in DiaAp (1.5), somewhat lower, but still positive in PartRecAp and RecAp (1.3 and 1.1 respectively) and weakly negative in VeinAp (0.9). Ratios of Y/Ho are highest in DiaAp and PartRecAp (average values 39 and 38, respectively) and slightly lower in RecAp and VeinAp (with an average value of 33 in both types).

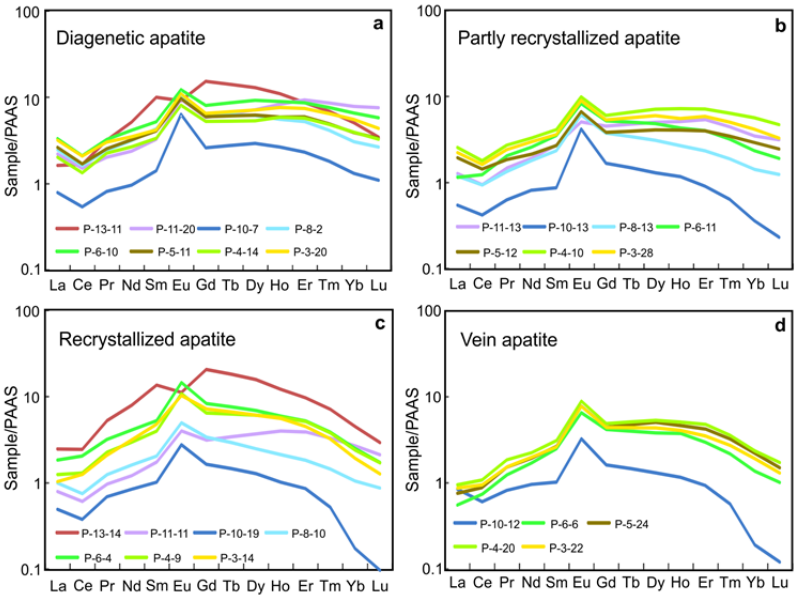

Figure 8. Post-Archean Australian Shale (PAAS) normalized REE patterns of apatite divided into four petrographic types: (a) Diagenetic apatite (b) Partly recrystallized apatite. (c) Recrystallized apatite. (d) Vein apatite. Each of the panels includes one representative REE pattern per sample. See sample locations in Joosu et al. (2015a – PAPER I) Figure 2.

Samples of the dolostone unit in the Shunga outcrop have the largest sample-scale variability. Similar to the lower mudstone unit, the REE patterns show LREE depletion (Figure 8). The average ratio of La_N/Sm_N in DiaAp, PartRecAp and RecAp is 0.5-0.6, but in VeinAp is somewhat higher reaching 0.8. Mid-REEs show a systematic trend of increasing Gd_N/Er_N values from DiaAp to PartRecAp to RecAp, except in the uppermost dolostone sample (P-11) where Gd_N/Er_N values are similar across the different types. Average Gd_N/Er_N values of DiaAp are close to one (flat MREE pattern) or slightly lower than one (ca 0.7). However, Gd_N/Er_N ratio values are up to 2.4 in RecAp. However in VeinAp a similar range of Gd_N/Er_N values was measured in only one sample of the dolostone interval (Figure 9).

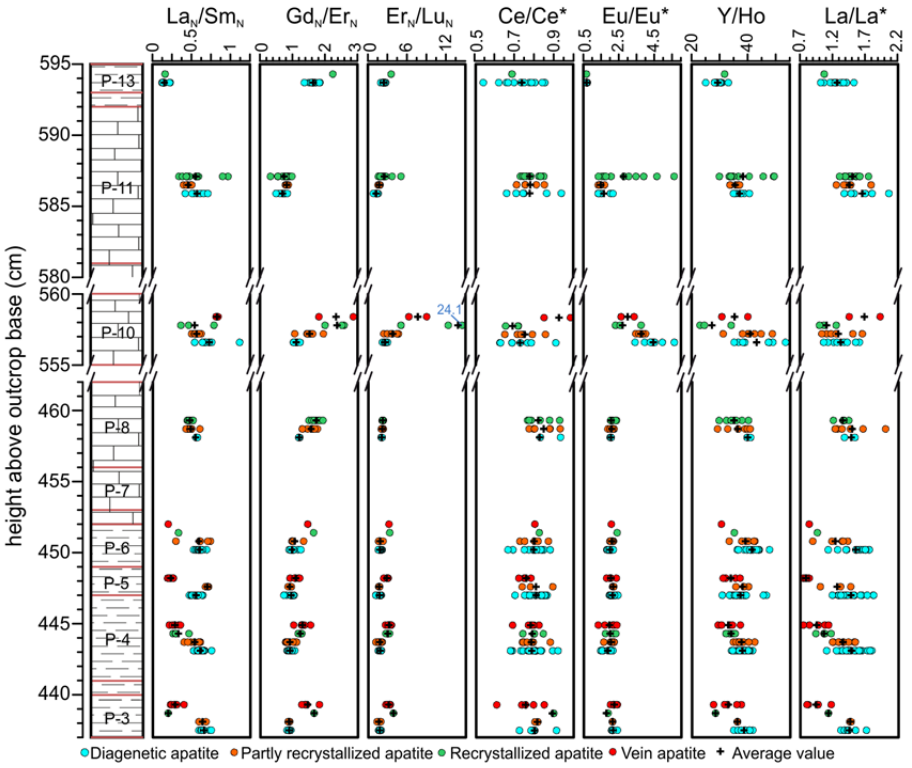

Figure 9. Stratigraphic profiles of selected apatite REE parameters for samples taken from the Shunga outcrop of the Zaonega Fm. The reported parameters for each sample are subdivided into four petrographic types. All individual determinations are reported as well as the average value (black cross) for each petrographic type.

In the dolostone unit, all apatite petrographic types have HREE patterns showing a depletion trend from Er_N to Lu_N (Joosu et al. 2105 – PAPER I). The Er_N/Lu_N values are relatively stable between the petrographic types at the base of the dolostone, highly variable with very strong HREE depletion in RecAp and VeinAp in the middle part of dolostone, and again less variable at the top of the unit. Cerium anomalies are uniformly negative and small, with average values of 0.8 in DiaAp, PartRecAp and RecAp, and slightly higher values around 0.9 in VeinAp. The Eu anomalies are positive and vary little between the petrographic types at the base of the dolostone where Eu/Eu* average values are 2.0–2.1. The middle part of the dolostone exhibits the strongest average Eu anomaly of the entire profile with 4.4 and 3.8 for DiaAp and PartRecAp and 2.7 and 3.0 for RecAp and VeinAp. The Eu anomaly at the top of dolostone is higher in RecAp (2.8) than in DiaAp (1.7) and PartRecAp (1.5). Samples from the middle of the dolostone unit however show an opposite trend. The La anomaly is positive in all samples with overlapping average La/La* values (1.4–1.7) regardless of petrographic type. The average Y/Ho ratio is somewhat

higher in DiaAp (41) than in PartRecAp (38), RecAp (36) and VeinAp (35) (Joosu et al. 2015a – PAPER I).

The upper mudstone unit has a different REE signature in comparison to other samples in this study (Figure 8). The REE patterns of DiaAp have strong MREE arching (average $La_N/Sm_N = 0.2$, $Gd_N/Er_N = 1.6$ and $Er_N/Lu_N = 2.5$). The RecAp has the same La_N/Sm_N as DiaAp, but Gd_N/Er_N and Er_N/Lu_N are higher (2.2 and 3.6, respectively). The Ce anomaly is negative with values slightly lower (0.7) than in underlying samples. In contrast to samples from the dolostone and lower mudstone units, the Eu anomaly is negative in DiaAp (0.7) and RecAp (0.6). The La/La* has positive values of 1.3 for DiaAp and 1.1 for RecAp. The Y to Ho ratio is lower than observed in other samples with average ratios of 29 and 32 for DiaAp and RecAp, respectively.

4.2. Ca-phosphate in Pilgujärvi Sedimentary Formation

4.2.1. Distribution and petrography of phosphate in Pilgujärvi SF

Phosphatic particles in Pilgujärvi SF are found in coarse-grained gritstones and sandstones composed of sub-rounded to rounded quartz(chert)-feldspar-schist grains (Figure 10). The P_2O_5 content in the samples studied varies between 1.5 and 3.9 wt.% and is mainly represented by (carbonate)-fluorapatite (Joosu et al. 2015b – PAPER IV). Three samples (AL05-P04, AL05-P06 and AL05-P07) representing pyritic gritstones are rich in pyrite and pyrrhotite and compose up to 35 wt.% of the crystalline phases. P-rich particles in the gritstone-sandstone samples occur typically as slab-shape elongated, sub-angular to rounded grains and occasionally as well rounded clasts. The typical size of phosphatic particles varies between 0.2 and 1.0 mm, but occasionally particles up to 5 mm in diameter can occur. Petrographically the phosphatic particles can be subdivided into four types that can co-occur in samples (Figure 11, Joosu et al. 2015b – PAPER IV). These petrographic types can be described as:

A. angular to sub-angular particles of massive, impurity-free, sub-micrometer size apatite crystal aggregates (AL05-PO4 and AL05-PO5);
B. elongated and sub-rounded particles of quartz-feldspar-mica/chlorite siltstone-shale or chert with pore-fillings of sub-micrometer crystal-size apatite cement(AL05-PO2 and AL05-PO5);
C. sub-angular to rounded particles of apatite aggregates with abundant quartz and feldspar, possibly transitional type between A and B type grains (AL05-PO2, AL05-PO4, AL05-PO5 and AL05-PO6);
D. sub-angular and angular apatite crystal aggregates with abundant pyrite (AL05-PO6).

Types A, B and C are found in all samples, but type D phosphatic clasts occur only in sample AL05-06. Some phosphatic particles show soft-deformation features (e.g. bending around quartz grains, Figure 10C) suggestive of a semi-lithified nature during re-deposition. Rare laminated shale particles, rich in apatite, were also found.

Apatite in different petrographic types occurs as fine-crystalline anhedral aggregates with uniformly fine crystallite size (<0.3 μm, Figure 11). Agglomerated 2–3 μm size spherical apatite aggregates composed of radially growing apatite crystallites were found in one phosphatic particle in sample AL05-P05.

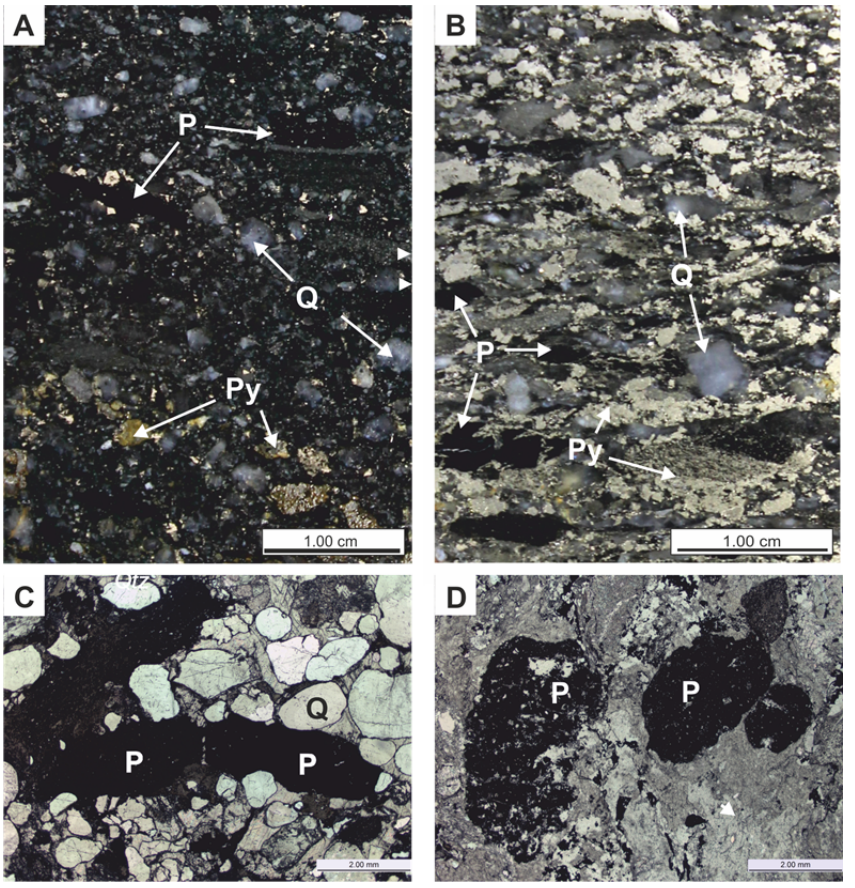

Figure 10. Optical reflected light images of the polished slabs from samples (A) AL05-P04 and (B) AL05-P07. Optical microscope images of phosphatic particles in thin sections (parallel nicols) from samples AL05-P05 (C) and AL05-P06 (D). N. Legend: P – phosphatic particle Q – quartz, Py – pyrite.

Pyrite in sulfide-rich samples (e.g. AL05-P06) occurs in a gritstone matrix as aggregates of euhedral pyrite grains, where the pyrite grains show weak zoning (see Figure 6b in Joosu et al. 2015b – PAPER IV). In phosphatic particles, pyrite occurs as xenomorphic-dendritic aggregates of fine/disseminated pyrite crystallites between the massive apatite areas. The pyritic areas in D-type phosphatic particles show indistinct banding-lamination. Pore-filling euhedral pyrite aggregates are possibly related to hydrothermal activity initiated by intrusion of

ferropicritic igneous rocks and synvolcanic Ni-Cu mineralization in the Pilgujärvi SF (Melezhik and Sturt 1994), whereas the pyrite within phosphatic particles is an early diagenetic sedimentary pyrite. Glenn and Arthur (1988) have shown that precipitation of pyrite and apatite in modern shelf phosphorites off the Peruvian coast appears to be coincident, while pyrite precipitation continues beyond that of apatite and it may replace the apatite, or infill remaining pore space after partial interstitial apatite cementation.

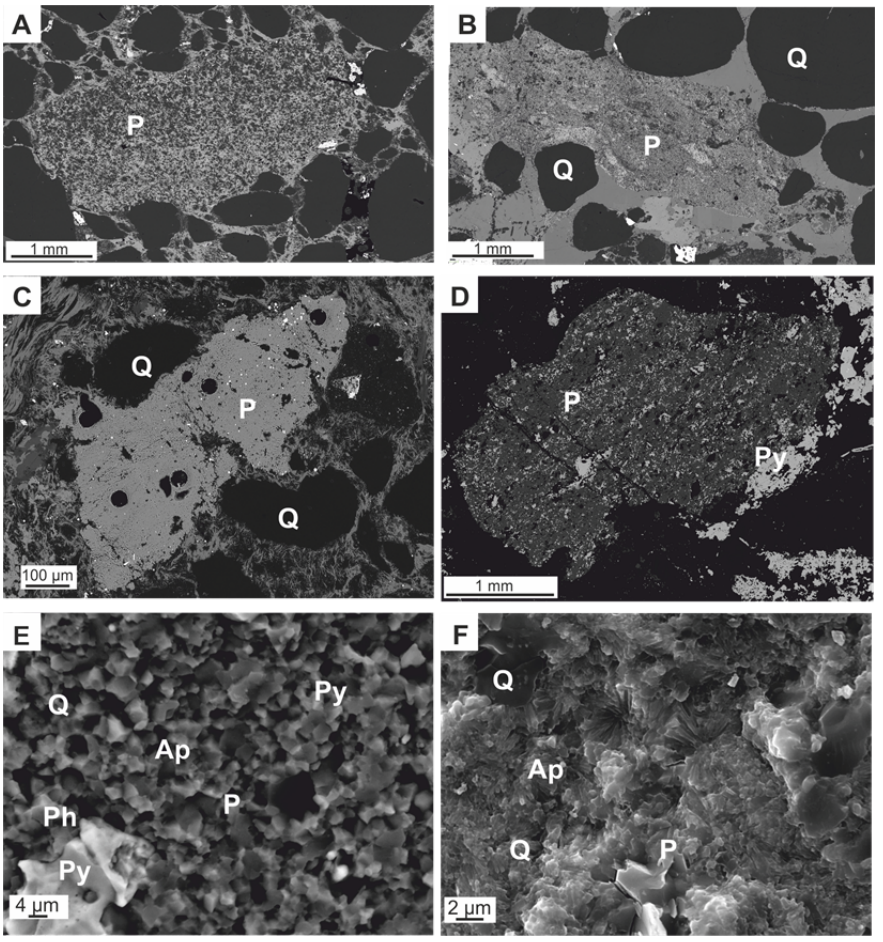

Figure 11. SEM BSE images of petrographic types of phosphatic aggregates in polished slabs of Pilgujärvi SF samples (A–D), (A) elongated and subrounded slabs of quartz-feldspar-mica/chlorite siltstone-shale or chert with pore-filling submicrometer crystal-size apatite cement (AL05-P04), (B) subangular to rounded phosphatic particles with abundant terrigenous phases (AL05-P05), (C) angular to subangular phosphatic particle consisting of massive apatite crystal aggregate (AL05-P04), (D) apatite crystal aggregate with abundant pyrite (AL05-P06), (E) phosphatic particles on broken surface in sample AL05-P06, (F) flower like apatite aggregates in sample A05-P05 (SE image). Legend: P – phosphatic particle, Q – quartz, Ph – phlogopite, Py – pyrite.

4.2.2. Rare Earth Element composition of apatite in Pilgujärvi SF

The REE analyses of apatite indicate a systematic variance of REE patterns across the different petrographic types of phosphatic particles (type A–D) (Figure 12, Joosu et al. 2015b – PAPER IV). The PAAS normalized REE patterns of particles comprising massive apatite crystal aggregates (type A, Figure 12) are characterized by a bell-shaped pattern with elevated MREEs (Gd_N to Er_N), and depleted LREEs (La_N to Sm_N) and even more depleted heavy HREEs (Er_N to Lu_N). The average La_N/Sm_N ratio in apatite of this type is 0.5 whereas the average Gd_N/Er_N ratio is 2.4, and Er_N/Lu_N 2.4. Apatite REE patterns of type B particles (where apatite occurs as a cementing matrix) are flatter (Figure 12), but also show enrichment in MREEs with a distinct positive Eu anomaly and in some cases a weak positive Ce anomaly. Some apatite REE patterns of type B clasts are similar to patterns in type A clasts with clearly emerging MREE enrichment.

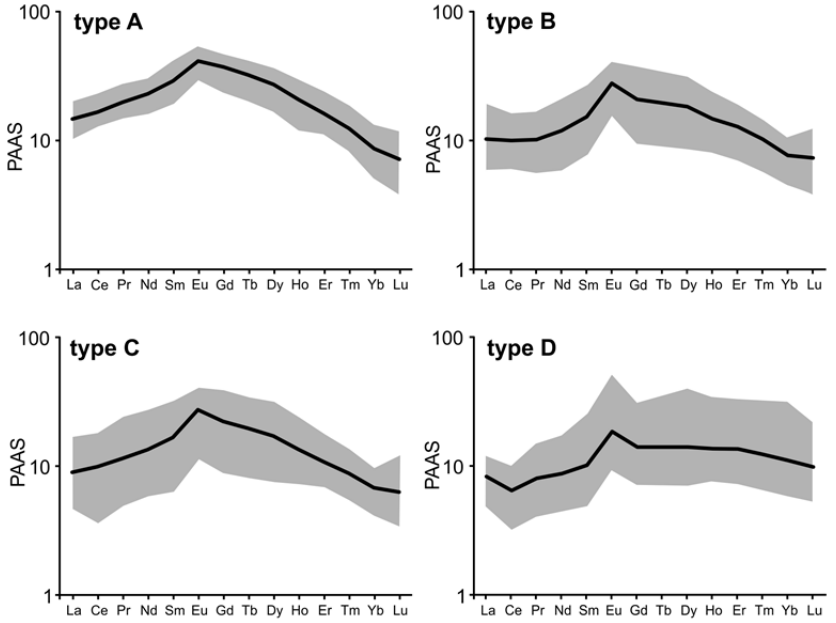

Figure 12. Post-Archean Australian Shale (PAAS) normalized REE patterns of apatite in phosphatic particles of different petrographic types in Pilgujärvi SF. The black line shows the average value of each petrographic type and gray shading shows the variation.

The La_N/Sm_N, Gd_N/Er_N and Er_N/Lu_N values of type B are 0.7, 1.6 and 1.8, respectively. Clasts of type C that petrographically are transitional between types A and B also have mixed/intermediate REE patterns with characteristics of both A and B types (Figure 12). The average La_N/Sm_N, Gd_N/Er_N and Er_N/Lu_N values of apa-

tite in C type clasts are 0.6, 2.0 and 1.8, respectively. In contrast, the REE patterns of the phosphatic particles rich in pyrite from pyritic gritstone sample (type D) have flat LREEs and MREEs, but show slightly depleted HREEs with an average La_N/Sm_N of 1, Gd_N/Er_N 1.1 and Er_N/Lu_N ratio of 1.4 (Joosu et al. 2015b – PAPER VI).

Values of the La anomaly fluctuate from negative to positive in all petrographic types and show no correlation with any specific type (Figure 13). The lowest average La/La* value is in type A (1.1) and is slightly higher in type C (1.2), while types B and D have a somewhat higher average La/La* at 1.3 and 1.4, respectively. Similarly, the Ce anomaly fluctuates from slightly negative to positive values within petrographic types (Figure 13a). The lowest average Ce/Ce* value is in type D (0.9) and highest in type B (1.1). The Eu anomaly is positive in all types, but shows slight differences between individual types (Figure 13b). The lowest average Eu/Eu* is in type A (1.3) whereas the average Eu/Eu* in type B is 1.6 and ca. 1.5 in both C and D types. In addition, there is a difference in the Y/Ho ratio between petrographic types (Figure 13c). Types A, B and C show average Y/Ho values of 32, 36 and 34, respectively, whereas the Y/Ho average of 46 in type D is statistically higher in comparison. The Y anomaly is absent in type A (average Y/Y* value 1.0) but is evident in type D (1.7). In types B and C the Y anomaly values are 1.2 and 1.1, respectively (Figure 13, Joosu et al. 2015b – PAPER IV).

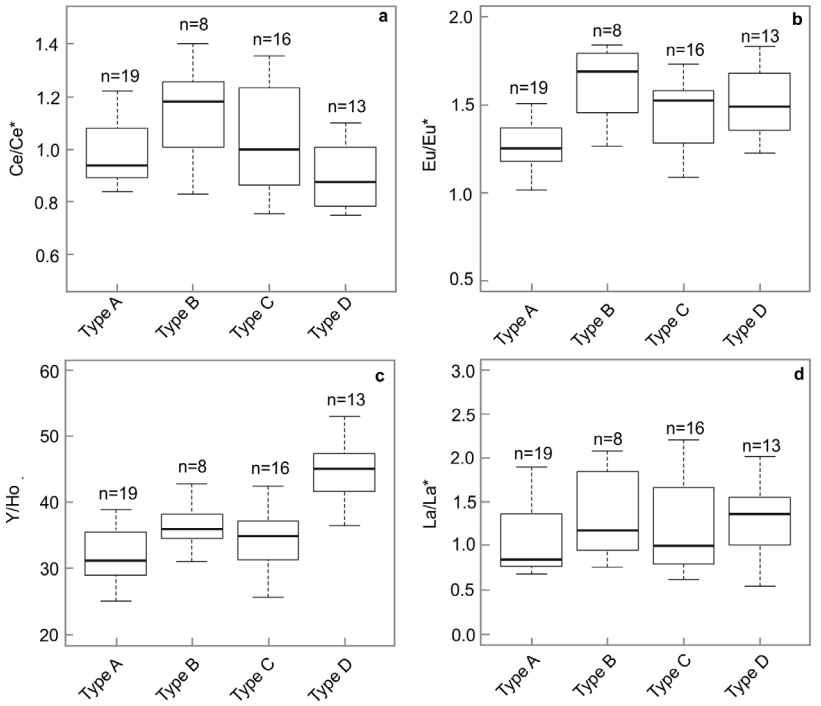

Figure 13. Apatite (a) Ce anomaly, (b) Eu anomaly, (c) Y/Ho ratio and (d) La anomaly variations in each petrographic type in Pilgujärvi SF.

5. DISCUSSION

5.1. Preservation of REE signal – diagenesis, hydrothermal overprint and weathering

Given the old age and greenschist facies metamorphic overprint on Zaonega and Pilgujärvi sedimentary sequences, recognition of sedimentary apatite with primary REE signatures requires careful assessment of post-depositional alteration processes that may have modified the primary signal. During late diagenesis and hydrothermal recrystallization, apatite typically becomes enriched in MREEs because of their preferential substitution for Ca in the apatite crystal lattice due to similarities in their ionic radii (Morad and Felitsyn 2001). Such crystal-structure controlled MREE enrichment mechanism is supported by the modeling studies of Reynard et al. (1999) who showed that MREE enrichment is expected during late diagenetic recrystallization whereas the adsorption by crystal surfaces during early diagenesis should lead to LREE enrichment. Consequently, the MREE behavior is considered as the most important characteristic to evaluate the effects of late diagenetic alteration of apatite. However, since MREE enrichment in sedimentary apatite is a widespread phenomenon, as documented by several studies (e.g. Bright et al. 2009; Chen et al. 2003; Felitsyn and Morad 2002; Mazumdar et al. 1999; Picard et al. 2002) it has been proposed that MREE enrichment may also be a result of other processes. Some authors argue that ancient seawater was MREE enriched and apatite with such REE patterns preserves a primary signal (e.g. Picard et al. 2002). Others have proposed that MREE enrichment in apatite occurs through the preferential uptake of MREEs by organisms in the water column and their subsequent release into pore water during organic matter degradation (e.g. Kidder and Eddydilek 1994).

An alternative explanation for MREE enrichment suggests that it can also result from apatite precipitation in depositional settings influenced by Fe(Mn)-oxyhydroxide redox-pumping and related adsorption-desorption of phosphate and REEs (Jarvis et al. 1994; Hailey et al. 2004). Hailey et al. (2004) demonstrated the occurrence of bell-shaped pore water REE profiles in a diagenetic Fe-oxide reduction zone in modern sediments on the Californian margin reflected in the signature of REEs adsorbed onto the Fe-oxides in the water column. Adsorbed REEs and phosphate are liberated to pore water during burial and reductive dissolution of freshly deposited Fe(Mn)-oxyhydroxides below the suboxic-anoxic redox boundary (Nelson et al. 2010), resulting in MREE enriched pore water (Hailey et al. 2004). Apatite precipitating in the Fe(Mn)-oxide reduction zone may thus show MREE enrichment and high average total REE concentrations.

The REE abundances, anomalies and normalized patterns of Diagenetic Apatite (DiaAp) and Partly Recrystallized Apatite (PartRecAp) in Zaonega Fm are broadly similar (Figure 8), indicating that partial recrystallization has caused insignificantly changes to the REE inventory of apatite. However, the REE

signatures of Recrystallized Apatite (RecAp) and Vein Apatite (VeinAp) in the same sequence are unique from DiaAp and PartRecAp REE patterns. RecAp and VeinAp in Zaonega Fm exhibit decreased ΣREEs and more pronounced MREE enrichment, consistent with expected crystal-structure driven REE changes during apatite recrystallization (Reynard et al. 1999). The MREE enrichment in apatite during recrystallization can also result from partitioning of LREEs and HREEs into the monazite and xenotime that have been detected in minor amounts within both the recrystallized apatite and vein apatite. This is also supported by the decrease of the Y anomaly in both RecAp and VeinAp, since xenotime has high Y abundance.

Positive Eu anomalies as seen in the lower mudstone unit and the lowermost dolostone sample of the Zaonega Fm are not affected by recrystallization, as shown by similar Eu/Eu* values across all petrographic types. However, DiaAp and PartRecAp from the middle part of the dolostone unit in Shunga outcrop exhibit the highest positive Eu anomalies (4.2 and 3.8 accordingly) and show a distinct Eu anomaly decrease during recrystallization (RecAp = 2.7 and VeinAp = 3.0). The opposite relationship however, is seen at the top of the dolostone unit where the Eu anomaly is higher, albeit very variable in RecAp (2.8) as compared to DiaAp (1.7) and PartRecAp (1.5). The Eu anomaly has been unaffected during recrystallization in the upper mudstone unit. The difference in the Eu anomaly between the DiaAp-PartRecAp and RecAp-VeinAp in the middle and upper dolostone unit can be explained by the involvement of external fluids during apatite recrystallization. These external fluids with positive Eu anomaly do not need to be supplied from distal sources since they can be formed by homogenizing the REE inventory derived during recrystallization from DiaAp in the middle (Eu/Eu* 4.2) and upper (Eu/Eu* 1.7) parts of the dolostone unit. It is evident from petrographic and REE characteristics that DiaAp in Zaonega Fm rocks exposed at the Shunga outcrop carries the best-preserved REE signature though bearing notable MREE enrichment (see Figure 8).

Similar to Zaonega Fm diagenetic apatite, the A, C and some B-type particles in Pilgujärvi SF show bell-shape MREE enriched patterns (Figure 11). In Pilgujärvi SF the MREE enrichment is less pronounced in B-type particles and nearly absent in D-type; the last being characterized by positive Eu anomalies and flat MREE and HREE patterns. Nevertheless, the La_N/Sm_N ratios fall within the range of modern seawater in the Zaonega Fm DiaAp and Pilgujärvi SF B- and D-type apatitic particles, whereas in A- and C-types the La_N/Sm_N ratios are mostly lower than typical seawater values. The somewhat elevated La_N/Yb_N ratios in all petrographic types of phosphatic particles in Pilgujärvi SF and in Zaonega Fm compared to modern seawater values may be indicative of the adsorption of LREEs on crystal surfaces, possibly during early digenesis. It is important to note that apatite in D-type particles from Pilgujärvi SF seems to have preserved the most seawater-like pattern as also evidenced by La_N/Yb_N and La_N/Sm_N ratios.

In contrast to Zaonega Fm, the phosphatic particles of the Pilgujärvi SF are not *in situ* but have been eroded, transported and redeposited in a deltaic

environment (Bekasova 1985) that implies a possible weathering imprint on apatite REE composition. Shield and Stille (2001) have proposed that REEs tend to escape during weathering because surface waters have low concentration of REEs compared to apatite. During weathering La, Gd and Y should be preferentially retained in apatite due to a tetrad effect (Bau and Dulski 1996). As a consequence, Y/Y* and La_N/Nd_N should increase during weathering (Shields and Stille 2001) resulting in a positive correlation between Y anomaly and La_N/Nd_N. In Pilgujärvi SF samples, a positive covariance between Y/Y* and La_N/Nd_N is particularly evident in A-type clasts (see Figure 10b in Joosu et al. 2015b – PAPER IV). However, digenetic recrystallization processes can also produce a positive Y/Y* versus La_N/Nd_N relationship (Reynard et al. 1999). Furthermore, the grain-clasts of the Pilgujärvi SF P-rich gritstone contain well preserved sedimentary pyrite (Figure 11), which suggests that clasts cannot have been influenced, at least significantly, by weathering. Nevertheless, some particles, including those pyrite was preserved intact within their interior, have thin Fe-oxide grain-coatings (see Figure 11 in Joosu et al. 2015b – PAPER IV) and decreasing pyrite abundance gradients toward the edge of the particles (Lepland et al. 2013 – PAPER III), implying either reworking in surface processes or influence of percolating meteoric waters.

5.2. Paleoenvironmental setting of the Paleoproterozoic phosphogenesis in Onega Basin and Pechenga Greenstone Belt

Phosphogenesis in modern seas is tied to upwelling in shelf environments, for example along the Namibian coast, the South African west coast and in the Arabian Sea. These areas are characterized by high biological production (Föllmi 1996) and varying anoxic-suboxic redox conditions where phosphate concentration/precipitation occurs through bacterially mediated redox-processes within the pore space of suboxic sediments in close proximity to the sediment – water interface (Arning et al. 2008).

The REE patterns of authigenic apatite are widely used to characterise the redox chemistry of ancient oceans (e.g. Wright et al. 1987). However, biologically precipitated apatite is a thermodynamically unstable, hydroxyapatite-like, poorly crystalline phase (Neary et al. 2011) that is readily recrystallized during diagenesis (Trueman 2013). Consequently, biogenic (hydroxyl-)apatite has been shown to be a highly ambiguous carrier of information about primary redox conditions, specifically due to recrystallization and adsorption effects (e.g. Herwartz et al. 2013). In contrast, the sedimentary carbonate-fluor apatite (Knudsen and Gunter 2002) is a thermodynamically stable apatite phase in solutions with elevated bi-carbonate anion activity, such as seawater (Jahnke 1984). Therefore, in the absence of a thermodynamic driver for recrystallization, the sedimentary apatite could be considered as a stable phase and the

REE composition of authigenic sedimentary apatite may parallel the ambient water conditions at the time and location of precipitation (Piper and Bau 2013).

5.2.1. Ce anomaly

In particular, the Ce anomaly in apatite is considered as a proxy for the sedimentary environment oxidation state (Liu et al. 1988). A Ce anomaly should not appear in authigenic sedimentary phases when the water column remains fully reducing and has been shown to have been absent in seawater prior to the GOE at ca. 2.3 Ga (Planavsky et al. 2010). In oxygenated and circulating modern oceans, Ce is removed from the water column by Fe-Mn oxyhydroxides, giving a negative Ce anomaly. In stratified water-bodies with well-developed redoxclines (e.g. the Black Sea), negative Ce anomalies become increasingly negative with depth until reaching the redoxcline, where it sharply diminishes due to reduction of Ce^{4+} to a soluble Ce^{3+} as the environment becomes anoxic and euxinic (Ling et al. 2013). In addition to oxidation state, Ce depletion in seawater is affected by microbial activity that catalyzes oxidation of Ce^{3+} (Moffett 1990), pH of the water, water depth and age of the seawater body, and therefore Ce behavior should be interpreted with caution (Pattan et al. 2005; Shields and Stille 2001). The Ce anomalies recorded in the Zaonega Fm DiaAp are consistently moderately negative throughout the sampled interval (Joosu et al. 2015a – PAPER I) indicating that the sedimentary basin water column was at least partly oxic allowing Ce oxidation and removal. This is supported by high, albeit variable, abundances of redox-sensitive Mo and U in the upper, P- rich part of the Zaonega Fm, this can be interpreted as the result of fluctuating redox states and episodes of oxic conditions (Lepland et al. 2014 – PAPER II). In Pilgujärvi SF the Ce anomaly fluctuates from slightly negative to positive in all petrographic types, though the Ce/Ce* values are mostly negative in D-type particles suggest similar fluctuating redox conditions at shallow sediment depth below the sediment-water interface during apatite precipitation as in Zaonega Fm. Positive Ce/Ce* values in Pilgujärvi SF apatites are probably the effect of a shifted (fluctuating) redox boundary that results in Ce remobilization from sediments and reductively dissolving Fe-Mn oxyhydroxides under anoxic conditions resulting in increased Ce concentrations in pore water. Wright et al. (1987) have shown that while Ce/Ce* values of authigenic apatite are strongly negative in deep ocean sediments, apatite deposited in high primary productivity regions on modern continental shelves (Peru, Namibia) are specifically characterized with Ce/Ce* values that are positive or only slightly negative, reflecting a suboxic-to-anoxic state of the sea-bottom environment.

5.2.2. Eu anomaly

The Eu anomaly in the Pilgujärvi SF apatite is positive in all petrographic types, varying from approximately 1.0 to 1.84 (Joosu et al. 2015b – PAPER IV) but in

Zaonega Fm while the Eu anomaly is positive in the lower mudstone and dolostone units it is negative in the upper mudstone unit (Joosu et al. 2015a – PAPER I). Europium is a redox sensitive element that does not fractionate under normal surface conditions. However, under extremely reducing and/or high temperature (>200 °C) environments it is reduced to mobile Eu^{2+}. Europium anomalies are therefore commonly observed in hydrothermal fluids and venting site sediments and even in shells of organisms inhabiting these sites (Bau et al. 2010). These anomalies can be positive (Bau et al. 2010; Michard et al. 1993) as well as negative (Bach et al. 2003). Unlike with Ce/Ce*, the Eu anomaly recorded in authigenic apatite is considered to be a stable tracer that does not change during diagenesis, except under extremely reducing conditions in environments where sulfate reduction has gone to completion (Mazumdar et al. 1999; Shields and Stille 2001). Positive Eu/Eu* values both in Zaonega Fm and Pilgujärvi SF phosphatic particles can be attributed to a hydrothermal influence. Both basins (Onega and Pechenga) were magmatically active and comprise numerous mafic (also ultramafic in Pilgujärvi SF) sills and lava flows. These sills and lava flows gave rise to hydrothermal activity, seepage/venting and hydrocarbon formation/migration (Črne et al. 2013; Qu et al. 2012; Melezhik and Hanski 2013) that influenced water chemistry in the vicinity of venting sites and around the margins of intrusions. The variable Eu anomaly in Pilgujärvi SF apatitic particles (Joosu et al. 2015b – PAPER IV) could be indicative of the formation of the original P-rich sediment at different proximities to the venting sites and/or a changing influence of the magmatic/hydrothermal discharges during deposition. The P-rich sediments deposited closer to venting sites or during higher magmatic activity could be indicated by higher Eu anomaly values than the those precipitated at some distance from vents or during periods of lower magmatic activity (e.g. Bau et al. 2010).

Interestingly, the apatite in the upper mudstone unit in Zaonega Fm shows a change in Eu behavior as the positive anomaly observed in the underlying lower mudstone and dolostone units is replaced by a negative Eu anomaly (Joosu et al. 2015a – PAPER I), which is rarely seen in authigenic apatites (Shields and Stille 2001). Although hydrothermal vents are known to carry occasional negative Eu anomalies it is rather rare. The upper mudstone unit is overlain by a >6 m thick dolostone-chert interval (see Figure 2 in Joosu et al. 2015a – PAPER I). Cherts in this interval have transitional, replacive contacts with dolostone, hence it appears likely that the cherts were formed due to silica mobility and veining involving relatively high-temperature fluids. Chert veins are not found below the dolostone-chert interval in the Shunga outcrop, suggesting that fluid flow controlling silica mobility was largely lateral in this particular area. These fluids may have affected the underlying upper mudstone unit and it is proposed that the original REE signatures in the upper mudstone were modified during fluid reworking, the negative Eu/Eu* values are a result of Eu leaching under reducing conditions. This hypothesis is supported by the evidence of MREE enrichment reflecting a strong secondary overprint of REE patterns that is not seen in underlying samples. Since carbonate sediments lithify rapidly in

comparison to mudstone, it appears possible that the dolostone unit between the upper and lower mudstones had already become lithified during the formation of the dolostone-chert interval, and thus the dolostone provided effective shielding against fluid alteration from above.

5.2.3. Y/Ho behavior

Yttrium behavior in apatite is similar to that in redox-insensitive REEs, especially holmium, that has identical valence and similar ionic radii. Therefore Y and Ho behave similarly in many geochemical processes, resulting in a constant chondritic weight-ratio Y/Ho = 28 in igneous rocks (Bau and Dulski 1996) and in hydrothermal fluids (Bau and Dulski 1999). In modern seawater superchondritic Y/Ho values are measured with a typical weight-ratio above 52 (Nozaki et al. 1997), since in oxygenated seawater REEs are more Fe–Mn particle reactive than Y (Bau and Dulski 1994).

The DiaAp from the lower mudstone and dolostone unit of the Zaonega Fm in Shunga outcrop has an average Y/Ho ratio of around 40, but this drops to 30 in the upper mudstone unit (Joosu et al. 2015a – PAPER I). These values suggest that DiaAp in the lower mudstone unit and in the dolomite unit from Zaonega Fm was precipitated from seawater exhibiting modern-type Y/Ho behavior. Y/Ho values are even higher in the apatite in type D particles (average 46) from Pilgujärvi SF (Joosu et al. 2015b – PAPER IV), which also suggests phosphate precipitation in equilibrium with a fluid whose REE and Y composition was similar to modern oxygenated seawater, possibly at shallow depth. This interpretation is further supported by the Ce anomaly values that are mostly negative in D-type particles, suggesting Ce fractionation in a slightly oxygenated environment.

The low Y/Ho ratios (<40) in the upper mudstone unit in Shunga outcrop of Zaonega Fm and A-, B- and C-type apatite particles in Pilgujärvi SF, suggest either hydrothermal influence or precipitation within sediments deposited at greater depths. Alternatively, it might indicate a secondary overprint, as the Y/Ho values in DiaAP in Zaonega Fm are similar to recrystallized and vein apatite Y/Ho in underlying units in Shunga outcrop (Joosu et al. 2015a – PAPER I).

5.2.4. Paleoenvironmental implications

The environmental conditions recorded in the sedimentary apatite from Zaonega Fm of Onega basin and Pilgujärvi SF of Pechenga basin can be interpreted as similar. The most pristine sedimentary diagenetic apatite in the Zaonega Fm shares similar characteristics with D-type apatite in the Pilgujärvi SF. For example the negative Ce anomaly (0.6–0.9) in Zaonega Fm and fluctuating in Pilgujärvi SF (0.8–1.1) suggests precipitation in suboxic conditions below the seawater-sediment interface (Joosu et al. 2015a – PAPER I). Such environ-

mental conditions are favorable for sulfur metabolizers that control the phosphogenesis in modern sediments (Schulz and Schulz 2005; Arning et al. 2009). Sulfate reducers thrive in anoxic environments where organic matter and sulfate is abundantly available while reduced Fe is limited (Alsenz et al. 2015). Moreover, in sediments with sharp redoxcline, the presence of sulfate reducers is closely associated with sulfur-oxidizing bacteria that inhabit diagenetic zones with periodically fluctuating (sub)oxic-sulfidic conditions and gain energy from the oxidation of H_2S and other reduced-sulfur species using O_2 or NO_3^-.

Modern phosphogenic areas are closely linked with continental shelf environments where upwelling of nutrient rich, deep-ocean water facilitates high biological production (Föllmi 1996). Fluctuating anoxic-suboxic redox conditions and redox dependent microbial processes within the sediment pore space leads to elevated phosphate concentrations resulting in apatite precipitation (Schulz and Schulz 2005). More specifically, Arning et al. (2009) show that phosphatic laminites forming at suboxic bottom water conditions in modern upwelling areas off Peru are characterized by a slightly negative Ce anomaly as seen in the best preserved apatite in Paleoporoterozoic Zaonega Fm in Onega basin and Pilgujärvi SF in Pechenga basin.

Positive Eu anomalies in apatite from the Pilgujärvi SF and the Zaonega Fm suggest an influence of hydrothermal fluids during apatite formation that is consistent with the magmatically active setting of both basins (Črne et al. 2013, Hanski et al. 2014). One significant difference between the two localities is that the Zaonega Fm phosphatic lenses and nodules formed *in situ* in contrast to the re-deposited P-rich particles in the Pilgujärvi SF. Phosphatic particles are not widespread throughout the Pilgujärvi SF, but occur specifically in the center of the formation in coarse-grained beds at the base of the rhythmically interbedded gritstone- sandstone-shale sequence: they are interpreted as the proximal facies to a submarine fan delta (Akhmedov and Krupenik 1990; Melezhik et al. 1998). Lepland et al. (2013 – PAPER III) have pointed out that gravel sized angular to rounded phosphatic grains showing soft-sediment deformation features cannot have been transported over long distances and are possibly derived locally. Abundant angular-subangular P-rich particles along with deformed mudstone clasts suggest transportation mainly by sediment gravity flows rather than in bedload. This indicates that slumping in the upper part of the shallow shelf was probably the main sediment source for the coarse-grained sediments in the submarine fan-delta slope, which were then deposited in troughs downslope from the slump scar (e.g. Postma 1984). This interpretation suggests that different types of apatitic particles were derived from a rather restricted area of the shallow marine shelf plateau directly above the fan-delta complex, which is a typical site for phosphogenesis along modern shelf margins too (Föllmi 1996). Deposits of Zaonega Fm in Onega basin containing sedimentary apatite possibly represent such depositional accumulations at the margin of the rifted Karelian craton.

6. CONCLUSIONS

This thesis focused on petrographic and geochemical characterization and Rare Earth Element (REE) analysis of sedimentary phosphate phase (apatite) in ca 2 Ga Paleoproterozoic Onega and Pechenga basins, Russia. The aim of the thesis was to reveal the environmental conditions of the phosphogenesis in these basins with an emphasis on the redox state of the water column and pore-fluid at shallow sediment depths. The central hypothesis was proposed that Paleoproterozoic phosphogenesis was triggered by the Great Oxygenation Event at ca 2.3 Ga that lead to the rise in dissolved oxygen content of the oceans and build-up of sulfate concentrations to levels allowing establishment of (sub)oxic-sulfidic redoxclines at shallow sediment depths and thus facilitating sedimentary apatite precipitation. Similar fluctuating (sub)oxic-sulfidic redoxclines exist in modern upwelling areas for example along the Namibian coast, the South African west coast and in the Arabian Sea, where phosphate concentration and precipitation occurs through microbially influenced redox-processes within the pore space of suboxic sediments in close proximity to the sediment–water interface.

Apatite in Zaonega Formation of the Onega basin occurs as impure laminae, lenses and round-oval nodules and is typically interweaved with organic matter. Within those the apatite occurs predominantly as cylindrical aggregates/ particles imprinted into the matrix of organic matter and the phlogopite. The cylinders have been variably recrystallized with the best preserved end-member consisting of nanometer scale crystallites intergrown with finely dispersed organic matter and the most altered end-member forming a cylindrical single crystal of apatite. Based on REE patterns, the best preserved diagenetic apatite can be shown to be largely (or completely) unaffected recrystallization or weathering, suggesting REE signatures reflect pore water REE composition during apatite precipitation. The PAAS normalized REE patterns of this diagenetic apatite typically have moderately negative Ce anomalies, and positive Eu anomalies. The negative Ce anomalies, it is suggested, result from partial oxygenation of the water column resulting in oxidation of Ce and its subsequent removal by Fe-Mn oxides. The positive Eu anomalies indicate an influence of Eu enriched hydrothermal fluids during apatite precipitation in this magmatically active basin, however, negative values in the uppermost part of the studied section of the Zaonega Formation mudstone-dolostone sequence are presumed to be the result of diagenetic leaching under extremely reducing conditions induced by late diagenetic fluid circulation.

In contrast to mostly *in situ* phosphatic particles in Zaonega Formation, Onega Basin; the Pilgujärvi Sedimentary Formation of the Pechenga basin (Greenstone Belt) contains redeposited phosphatic sand-to-gravel/pebble sized particles. They were transported and re-deposited in a hydrothermally influenced, deltaic or deep-water continental slope turbidite fan environment. According to petrographic characteristics, the phosphatic sediment particles can be subdivided into four different types. Each type has a different REE signature

possibly reflecting the diagenetic conditions during the apatite precipitation rather than late diagenetic recrystallization and/or metamorphic overprint after the turbidite deposition, in as much as the different types co-exist within the same sample. The REE signal in type D apatitic particles that are evidently the best preserved shows slightly negative Ce anomaly that can be interpreted to reflect partial seawater oxygenation. On the other hand, positive Eu/Eu* values can be attributed to hydrothermal venting that is consistent with the magmatically active setting of the basin.

The environmental conditions of the phosphogenesis recorded in apatite in the Paleoproterozoic Pilgujärvi Sedimentary Formation of the Pechenga basin and in Zaonega Formation, Onega basin are alike suggesting that the phosphogenic events in these sedimentary basins occurred in a similar way. Initiation of the phosphogenesis in these basins possibly marks the development of specific anoxic(sulfidic)-suboxic redoxclines at shallow sediment depth during the Paleoproterozoic that are very similar to the environmental settings found in modern phosphogenic areas. Also, it is important to notice that the phosphogenic events in Onega and Pechenga basins (estimated ages 1.97 Ga and 1.92 Ga, respectively) are delayed by ca. 300–400 Ma from the Great Oxygenation Event (ca. 2.3 Ga) suggesting that some time was needed to establish redoxcline conditions suitable for concentration of interstitial phosphate in shallow sediments on the sea bed. However, this hypothesis needs testing in other Paleoproterozoic phosphorite bearing sequences.

REFERENCES

Akhmedov, A.M., Krupenik, V.A., 1990. Turbiditic regime of sedimentation and pyrite formation in the Early Proterozoic Pechenga Basin. *Soviet Geology* 11, 51–60. (in Russian)

Alsenz, H., Illner, P., Ashckenazi-Polivoda, S., Meilijson, A., Abramovich, S., Feinstein, S., Almogi-Labin, A., Berner, Z., Püttmann, W., 2015. Geochemical evidence for the link between sulfate reduction, sulfide oxidation and phosphate accumulation in a Late Cretaceous upwelling system. *Geochemical Transactions* 16, 1–13

Amelin, Y.V., Heaman, L.M., Semenov, V.S., 1995. U-Pb Geochronology of Layered Mafic Intrusions in the Eastern Baltic Shield – Implications for the Timing and Duration of Paleoproterozoic Continental Rifting. *Precambrian Research* 75, 31–46.

Ammerman, J.W., Hood, R.R., Case, D.A., Cotner, J.B., 2003. Phosphorus deficiency in the Atlantic: An emerging paradigm in oceanography. *Eos, Transactions American Geophysical Union* 84, 165–170.

Arning, E.T., Birgel, D., Brunner, B., Peckmann, J., 2009a. Bacterial formation of phosphatic laminites off Peru. *Geobiology* 7, 295–307.

Arning, E.T., Birgel, D., Schulz-Vogt, H.N., Holmkvist , L., Jørgensen, B.B., Larson , A., Peckmann , J., 2008. Lipid biomarker patterns of phosphogenic sediments from upwelling regions. *Geomicrobiology Journal* 25, 69–82.

Arning, E.T., Lueckge, A., Breuer, C., Gussone, N., Birgel, D., Peckmann, J., 2009b. Genesis of phosphorite crusts off Peru. *Marine Geology* 262, 68–81.

Asael, D., Tissot, F.L.H., Reinhard, C.T., Rouxel, O., Dauphas, N., Lyons, T.W., Ponzevera, E., Liorzou, C., Chéron, S., 2013. Coupled molybdenum, iron and uranium stable isotopes as oceanic paleoredox proxies during the Paleoproterozoic Shunga Event. *Chemical Geology* 362, 193–210.

Bach, W., Roberts, S., Vanko, D.A., Binns, R.A., Yeats, C.J., Craddock, P.R., Humphris, S.E., 2003. Controls of fluid chemistry and complexation on rare-earth element contents of anhydrite from the Pacmanus subseafloor hydrothermal system, Manus Basin, Papua New Guinea. *Mineralium Deposita* 38, 916–935.

Bau, M., 1991. Rare-Earth Element Mobility during Hydrothermal and Metamorphic Fluid Rock Interaction and the Significance of the Oxidation-State of Europium. *Chemical Geology* 93, 219–230.

Bau, M., Balan, S., Schmidt, K., Koschinsky, A., 2010. Rare earth elements in mussel shells of the Mytilidae family as tracers for hidden and fossil high-temperature hydrothermal systems. *Earth and Planetary Science Letters* 299, 310–316.

Bau, M., Dulski, P., 1994. Evolution of the Yttrium-Holmium Systematics of Seawater Through Time. *Mineralogical Magazine* 58A, 61–62.

Bau, M., Dulski, P., 1996. Distribution of yttrium and rare-earth elements in the Penge and Kuruman iron-formations, Transvaal Supergroup, South Africa. *Precambrian Research* 79, 37–55.

Bau, M., Dulski, P., 1999. Comparing yttrium and rare earths in hydrothermal fluids from the Mid-Atlantic Ridge: implications for Y and REE behaviour during near-vent mixing and for the Y/Ho ratio of Proterozoic seawater. *Chemical Geology* 155, 77–90.

Bekasova, N.B., 1985. Pechenga (Kola Peninsula) paleogeography in early Pilgujärvi time of the early Proterozoic. *Lithology and Mineral Resources* 20, 127–137. (in Russian)

Bekasova, N.B., Dudkin, O.B., 1981. Composition and nature of early Precambrian Pechenga concretionary phosphorites (Kola peninsula). *Lithology and Mineral Resources* 6, 107–113. (in Russian)

Bekker, A., Holland, H.D., 2012. Oxygen overshoot and recovery during the early Paleoproterozoic. *Earth and Planetary Science Letters* 317, 295–304.

Bekker, A., Holland, H.D., Wang, P.L., Rumble, D., Stein, H.J., Hannah, J.L., Coetzee, L.L., Beukes, N.J., 2004. Dating the rise of atmospheric oxygen. *Nature* 427, 117–120.

Berner, R.A., 1973. Phosphate removal from sea-water by adsorption on volcanogenic ferric oxides. *Earth and Planetary Science Letters* 18, 77–86.

Bright, C.A., Cruse, A.M., Lyons, T.W., MacLeod, K.G., Glascock, M.D., Ethington, R.L., 2009. Seawater rare-earth element patterns preserved in apatite of Pennsylvanian conodonts? *Geochimica et Cosmochimica Acta* 73, 1609–1624.

Brock, J. and Schulz-Vogt, H.N., 2011. Sulfide induces phosphate release from polyphosphate in cultures of a marine Beggiatoa strain. *ISME Journal* 5, 497506.

Buseck, P.R., Galdobina, L.P., Kovalevski, V.V., Rozhkova, N.N., Valley, J.W., Zaidenberg, A.Z., 1997. Shungites: The C-rich rocks of Karelia, Russia. *Canadian Mineralogis*t 35, 1363–1378.

Chen, D.F., Dong, W.Q., Qi, L., Chen, G.Q., Chen, X.P., 2003. Possible REE constraints on the depositional and diagenetic environment of Doushantuo Formation phosphorites containing the earliest metazoan fauna. *Chemical Geology* 201, 103–118.

Črne, A.E., Melezhik, V.A., Prave, A.R., Lepland, A., Romashkin, A.E., Rychanchik, D.V., Hanski, E.J., Luo, Z., 2013. Zaonega Formation: FAR-DEEP Holes 12A and 12B, and neighbouring quarries. In: Melezhik, V.A., Prave, A.R., Fallick, A.E., Hanski, E.J., Lepland, A., Kump, L.R., Strauss, H. (Eds.). *Reading the Archive of Earth's Oxygenation.* Volume 2: *The Core Archive of the Fennoscandian Arctic Russia – Drilling Early Earth Project*. pp. 946–1007.

Felitsyn, S., Morad, S., 2002. REE patterns in latest Neoproterozoic-early Cambrian phosphate concretions and associated organic. *Chemical Geology* 187, 257–265.

Filippelli, G.M., 2002. The global phosphorus cycle. In: Kohn, M.J., Rakovan, J., Hughes, J.M. (Eds.). Reviews in mineralogy and geochemistry. Volume 48: *Phosphates: Geochemical, Geobiological, and Materials Importance*. pp. 391–425.

Filippelli, G.M., 2008. The global phosphorus cycle: Past, present, and future. *Elements* 4, 89–95.

Froelich, P.N., Bender, M.L., Luedtke, N.A., Heath, G.R., Devries, T., 1982. The Marine Phosphorus Cycle. *American Journal of Science* 282, 474–511.

Föllmi, K.B., 1996. The phosphorus cycle, phosphogenesis and marine phosphate-rich deposits. *Earth-Science Reviews* 40, 55–124.

Garnit, H., Bouhlel, S., Barca, D., Chtara, C., 2012. Application of LA-ICP-MS to sedimentary phosphatic particles from Tunisian phosphorite deposits: Insights from trace elements and REE into paleo-depositional environments. *Chemie Der Erde-Geochemistry* 72, 127–139.

Glenn, C.R., Arthur, M.A., 1988. Petrology and Major Element Geochemistry of Peru Margin Phosphorites and Associated Diagenetic Minerals – Authigenesis in Modern Organic-Rich Sediments. *Marine Geology* 80, 231–267.

Goldhammer, T., Bruchert, V., Ferdelman, T.G., Zabel, M., 2010. Microbial sequestration of phosphorus in anoxic upwelling sediments. *Nature Geoscience*, 3 557–561.

Gärtner, C., Bahlburg, H., Martin, A.P., Condon, D.J., Prave, A.R., Lepland, A., Berndt, J., Gerdes, A., 2011. Detrital zircon geochronology and provenance analysis for Paleoproterozoic siliciclastic sediments of the Fennoscandian Shield (extended abstract), IODP/ICDP Kolloquium, Münster, 14–16 March 2011, pp. 63–66.

Haley, B.A., Klinkhammer, G.P., McManus, J., 2004. Rare earth elements in pore waters of marine sediments. *Geochimica et Cosmochimica Acta* 68, 1265–1279.

Hannah, J.L., Stein, H.J., Zimmerman, A., Yang, G., Markey, R.J., Melezhik, V.A., 2006. Precise 2004 ± 9 Ma Re–Os age for Pechenga black shale: Comparison of sulfides and organic material. *Geochimica et Cosmochimica Acta* 70, A228.

Hannah, J.L., Stein, H., Yang, G., Zimmerman, A., Melezhik, V., Filippov, M., Turgeon, S., Creaser, R., 2008. Re-Os geochronology of a 2.05 Ga fossil oil field near Shunga, Karelia, NW Russia, the 33rd International Geological Congress, Oslo, Norway.

Hannah, J.L., Stein, H.J., Yang, G., Zimmerman, A., 2010. Paleoproterozoic pyrobitumen: Re-Os goechemistry reveals the fate of giant carbon accumulations in Russian Karelia, Fall Meeting, AGU, San Francisco, USA.

Hanski, E.J., Huhma, H., Melezhik, V.A., 2014. New isotopic and geochemical data from the Palaeoproterozoic Pechenga Greenstone Belt, NW Russia: Implication for basin development and duration of the volcanism. *Precambrian Research* 245, 51–65.

Hanski, E.J., Huhma, H., Smol'kin, V.F., Vaasjoki, M., 1990. The age of ferropicritic volcanites and comagmatic Ni-bearing intrusions at Pechenga, Kola Peninsula, U.S.S.R. *Geol Surv Finland Bull* 62, 123–133.

Herwartz, D., Tutken, T., Jochum, K.P., Sander, P.M., 2013. Rare earth element systematics of fossil bone revealed by LA-ICPMS analysis. *Geochimica et Cosmochimica Acta* 103, 161–183.

Jahnke, R.A., 1984. The Synthesis and Solubility of Carbonate Fluorapatite. *American Journal of Science* 284, 58–78.

Jarvis, I., Burnett, W.C., Nathan, Y., Almbaydin, F.S.M., Attia, A.K.M., Castro, L.N., Flicoteaux, R., Hilmy, M.E., Husain, V., Qutawnah, A.A., Serjani, A., Zanin, Y.N., 1994. Phosphorite Geochemistry-State-of-the-Art and Environmental Concerns. *Eclogae Geologicae Helvetiae* 87, 643–700.

Jochum, K.P., Weis, U., Stoll, B., Kuzmin, D., Yang, Q.C., Raczek, I., Jacob, D.E., Stracke, A., Birbaum, K., Frick, D.A., Gunther, D., Enzweiler, J., 2011. Determination of Reference Values for NIST SRM 610-617 Glasses Following ISO Guidelines. *Geostandards and Geoanalytical Research* 35, 397–429.

Joosu, L., Lepland, A., Kirsimäe, K., Romashkin, A.E., Roberts, N.M.W., Martin, A.P., Črne, A.E., 2015a The REE-composition and petrography of apatite in 2 Ga Zaonega Formation, Russia: The environmental setting for phosphogenesis. *Chemical Geology* 395, 88–107.

Joosu, L., Lepland, A., Kreitsmann, T., Üpraus, K., Roberts, N.M.W., Paiste, P., Martin, A.P., Kirsimäe, K., 2015b Petrography and the REE-composition of apatite in the Paleoproterozoic Pilgujärvi Sedimentary Formation, Pechenga Greenstone Belt, Russia. Manuscript submitted to G*eochimica et Cosmochimica Acta*.

Kent, A.J.R., Ungerer, C.A., 2005. Production of barium and light rare earth element oxides during LA-ICP-MS microanalysis. *Journal of Analytical Atomic Spectrometry* 20, 1256–1262.

Kidder, D.L., Eddydilek, C.A., 1994. Rare-Earth Element Variation in Phosphate Nodules from Midcontinent Pennsylvanian Cyclothems. *Journal of Sedimentary Research* Section a-*Sedimentary Petrology and Processes* 64, 584–592.

Knudsen, A.C., Gunter, M.E., 2002. Sedimentary phosphorites – An example: Phosphoria formation, southeastern Idaho, USA. In: Kohn, M.J., Rakovan, J., Hughes, J.M. (Eds.). Reviews in mineralogy and geochemistry. Volume 48: *Phosphates: Geochemical, Geobiological, and Materials Importance*. pp. 363-389.

Koutsoukos, P.G. and Valsami-Jones, E., 2004. Principles of phosphate dissolution and precipitation. In: Valsami-Jones, E. (Ed.). *Phosphorus in Environmental Technologies, Principles and Applications*. pp. 195–248.

Koistinen, T., Stephens, M.B., Bogatchev, V., Nordgulen, Ø., Wenneström, M., Korhonen, J., (Comps.), 2001, Geological Map of the Fennoscandian Shield, Scale 1:2 000 000, Espo, Trondheim, Upsala, Moscow.

Krajewski, K.P., Vancappellen, P., Trichet, J., Kuhn, O., Lucas, J., Martinalgarra, A., Prevot, L., Tewari, V.C., Gaspar, L., Knight, R.I., Lamboy, M., 1994. Biological processes and apatite formation in sedimentary environments. *Eclogae Geologicae Helvetiae* 87, 701–745.

Kump, L., 2008. The rise of atmospheric oxygen. *Nature* 453, 277–278.

Lepland, A., Joosu, L., Kirsimäe, K., Prave, A.R., Romashkin, A.E., Crne, A.E., Martin, A.P., Fallick, A.E., Somelar, P., Upraus, K., Mand, K., Roberts, N.M.W., van Zuilen, M.A., Wirth, R., Schreiber, A., 2014. Potential influence of sulphur bacteria on Palaeoproterozoic phosphogenesis. *Nature Geoscience* 7, 20–24.

Lepland, A., Melezhik, V.A., Papineau, D., Romashkin, A.E., Joosu, L., 2013. The earliest phosphorites: radical change in the phosphorus cycle during the Palaeoproterozoic. In: Melezhik, V.A., Prave, A.R., Hanski, E.J., Fallick, A.E.; Lepland, A., Kump, L. (Eds.). *Reading the Archive of Earth's Oxygenation*. Volume 3: *Global Events and the Fennoscandian Arctic Russia – Drilling Early Earth Project*. pp. 1275–1296.

Ling, H.F. et al., 2013. Cerium anomaly variations in Ediacaran-earliest Cambrian carbonates from the Yangtze Gorges area, South China: Implications for oxygenation of coeval shallow seawater. *Precambrian Research* 225, 110–127.

Liu, Y.G., Miah, M.R.U., Schmitt, R.A., 1988. Cerium – a Chemical Tracer for Paleo-Oceanic Redox Conditions. *Geochimica et Cosmochimica Acta* 52, 1361–1371.

Lyons, T.W., Reinhard, C.T., Planavsky, N.J., 2014. The rise of oxygen in Earth's early ocean and atmosphere. *Nature* 506, 307–315.

Martin, A.P., Condon, D.J., Prave, A.R., Melezhik, V.A., Lepland, A., Fallick, A.E., 2013. Dating the termination of the Palaeoproterozoic Lomagundi-Jatuli carbon isotopic event in the North Transfennoscandian Greenstone Belt. *Precambrian Research* 224, 160–168.

Martin, A. P., Prave, A. P., Condon, D. J., Lepland, A., Fallick, A. E., Romashkin, A. E., Medvedev, P. V., Rychanchik, D. V., 2015. Multiple Palaeoproterozoic Carbon Burial Episodes and Excursions. *Earth and Planetary Science Letters* 424, 226–236.

Mazumdar, A., Banerjee, D.M., Schidlowski, M., Balaram, V., 1999. Rare-earth elements and stable isotope geochemistry of early Cambrian chert-phosphorite assemblages from the Lower Tal formation of the Krol Belt (Lesser Himalaya, India). *Chemical Geology* 156, 275–297.

Mcarthur, J.M., Walsh, J.N., 1984. Rare-Earth Geochemistry of Phosphorites. *Chemical Geology* 47, 191–220.

Mclennan, S.M., 1989. Rare-Earth Elements in Sedimentary-Rocks – Influence of Provenance and Sedimentary Processes. *Reviews in Mineralogy* 21, 169–200.

Melezhik, V.A., Fallick, A.E., Filippov, M.M., Larsen, O., 1999. Karelian shungite – an indication of 2.0-Ga-old metamorphosed oil-shale and generation of petroleum: geology, lithology and geochemistry. *Earth-Science Reviews* 47, 1–40.

Melezhik, V.A., Fallick, A.E., Hanski, E.J., Kump, L., Lepland, A., Prave, A., Strauss, H., 2005. Emergence of the Modern Earth System during the Archean-Proterozoic Transition. *GSA Today* 15, 4–11.

Melezhik, V.A., Hanski, E.J., 2013. The Pechenga Greenstone Belt, in: Melezhik, V.A., Prave, A.R., Hanski, E.J., Fallick, A.E., Lepland, A., Kump, L.R., Strauss, H. (Eds.), *Reading the Archive of Earth's Oxygenation*. Volume 1: *The Paleoproterozoic of Fennoscandia as Context for the Fennoscandian Arctic Russia-Drilling Early Earth Project*. pp. 289–385.

Melezhik, V.A., Huhma, H., Condon, D.J., Fallick, A.E., Whitehouse, M.J., 2007. Temporal constraints on the Paleoproterozoic Lomagundi-Jatuli carbon isotopic event. *Geology* 35, 655–658.

Melezhik, V.A., Sturt, B.A., 1994. General Geology and Evolutionary History of the Early Proterozoic Polmak-Pasvik-Pechenga-Imandra Varzuga-Ustponoy Greenstone-Belt in the Northeastern Baltic Shield. *Earth-Science Reviews* 36, 205–241.

Melezhik, V.A., Sturt, B.A., 1998. The Early Proterozoic Pechenga-Varzuga Belt: a case of Precambrian back-arc spreading by Evgenii V. Sharkov and Valery F. Smolkin (1997) – *Precambrian Research* 82, 133–151: Comments. *Precambrian Research* 92, 215–218.

Michard, A., Michard, G., Stuben, D., Stoffers, P., Cheminee, J.L., Binard, N., 1993. Submarine Thermal Springs Associated with Young Volcanos – the Teahitia Vents, Society Islands, Pacific-Ocean. *Geochimica et Cosmochimica Acta* 57, 4977–4986.

Moffett, J.W., 1990. Microbially Mediated Cerium Oxidation in Sea-Water. *Nature* 345, 421–423.

Morad, S., Felitsyn, S., 2001. Identification of primary Ce-anomaly signatures in fossil biogenic apatite: implication for the Cambrian oceanic anoxia and phosphogenesis. *Sedimentary Geology* 143, 259–264.

Neary, M.T., Reid, D.G., Mason, M.J., Friscic, T., Duer, M.J., Cusack, M., 2011. Contrasts between organic participation in apatite biomineralization in brachiopod shell and vertebrate bone identified by nuclear magnetic resonance spectroscopy. *Journal of the Royal Society Interface* 8, 282–288.

Nelson, G.J., Pufahl, P.K., Hiatt, E.E., 2010. Paleoceanographic constraints on Precambrian phosphorite accumulation, Baraga Group, Michigan, USA. *Sedimentary Geology* 226, 9–21.

Nozaki, Y., Zhang, J., Amakawa, H., 1997. The fractionation between Y and Ho in the marine environment. *Earth and Planetary Science Letters* 148, 329–340.

Obersteiner, M., Peñuelas, P., Ciais, P., Velde, van der M., Janssens, I.A., 2013. The phosphorus trilemma. *Nature Geoscience* 6, 897–898.

Ovchinnikova, G.V., Kuznetsov, A.B., Melezhik, V.A., Gorokhov, I.M., Vasil'eva, I.M., Gorokhovskii, B.M., 2007. Pb-Pb age of Jatulian carbonate rocks: The Tulomozero Formation of Southeast Karelia. *Stratigraphy and Geological Correlation* 15, 359–372.

Papineau, D., 2010. Global Biogeochemical Changes at Both Ends of the Proterozoic: Insights from Phosphorites. *Astrobiology* 10, 165–181.

Partin, C.A., Bekker, A., Planavsky, N.J., Scott, C.T., Gill, B.C., Li, C., Podkovyrov, V., Maslov, A., Konhauser, K.O., Lalonde, S.V., Love, G.D., Poulton, S.W., Lyons, T.W., 2013. Large-scale fluctuations in Precambrian atmospheric and oceanic oxygen levels from the record of U in shales. *Earth and Planetary Science Letters* 369–370, 284–293.

Pattan, J.N., Pearce, N.J.G., Mislankar, P.G., 2005. Constraints in using Cerium-anomaly of bulk sediments as an indicator of paleo bottom water redox environment: A case study from the Central Indian Ocean Basin. *Chemical Geology* 221, 260–278.

Picard, S., Lécuyer, C., Barrat, J.–A., Garcia, J.–P., Dromart, G., Sheppard, S.M.F., 2002. Rare earth element contents of Jurassic fish and reptile teeth and their potential relation to seawater composition (Anglo-Paris Basin, France and England). *Chemical Geology* 186, 1–16.

Piper, D.Z., Bau, M., 2013. Normalized Rare Earth Elements in Water, Sediments, and Wine: Identifying Sources and Environmental Redox Conditions. *American Journal of Analytical Chemistry* 4, 69–83.

Planavsky, N., Bekker, A., Rouxel, O.J., Kamber, B., Hofmann, A., Knudsen, A., Lyons, T.W., 2010. Rare Earth Element and yttrium compositions of Archean and Paleoproterozoic Fe formations revisited: New perspectives on the significance and mechanisms of deposition. *Geochimica et Cosmochimica Acta* 74, 6387–6405.

Postma, G., 1984. Slumps and their deposits in fan delta front and slope. *Geology* 12, 27–30.

Puchtel, I.S., Arndt, N.T., Hofmann, A.W., Haase, K.M., KroÈner, A., Kulikov, K.S., Kulikova, V.V., Garbe-SchoÈnberg, C.-D., Nemchin, A.A., 1998. Petrology of mafic lavas within the Onega plateau, central Karelia: evidence for 2.0 Ga plume-related continental crustal growth in the Baltic Shield. *Contributions to Mineralogy and Petrology* 130, 134–153.

Puchtel, I.S., Brugmann, G.E., Hofmann, A.W., 1999. Precise Re-Os mineral isochron and Pb-Nd-Os isotope systematics of a mafic-ultramafic sill in the 2.0 Ga Onega plateau (Baltic Shield). *Earth and Planetary Science Letters* 170, 447–461.

Pufahl, P.K., Hiatt, E.E., Kurtis Kyser, T., 2010. Does the Paleoproterozoic Animikie Basin record the sulfidic ocean transition? *Geology* 38, 659–662.

Pufahl, P.K. and Hiatt, E.E., 2012. Oxygenation of the Earth's atmosphere-ocean system: A review of physical and chemical sedimentologic responses. *Marine and Petroleum Geology* 32, 1–20.

Qu, Y., Crne, A.E., Lepland, A., Van Zuilen, M.A., 2012. Methanotrophy in a Paleo-proterozoic oil field ecosystem, Zaonega Formation, Karelia, Russia. *Geobiology* 10, 467–478.

Reuschel, M., Melezhik, V.A., Whitehouse, M.J., Lepland, A., Fallick, A.E., Strauss, H.. 2012. Isotopic evidence for a sizeable seawater sulfate reservoir at 2.1 Ga. *Precambrian Research* 192, 78–88.

Reynard, B., Lecuyer, C., Grandjean, P., 1999. Crystal-chemical controls on rare-earth element concentrations in fossil biogenic apatites and implications for paleo-environmental reconstructions. *Chemical Geology* 155, 233–241.

Rozanov, A.Y., Astafieva, M.M., 2008. Prasinophyceae (green algae) from the Lower Proterozoic of the Kola Peninsula. *Paleontologicheskii Zhurnal* 4, 90–93.

Rozanov, A.Y., Astafieva, M.M., Hoover, R.B., 2007. Early Proterozoic (2.04 Ga) phoshorites of Pechenga Greenstone Belt and their origin. *Instruments, Methods, and Missions for Astrobiology* X, 6694.

Scott, C., Lyons, T.W., Bekker, A., Shen, Y., Poulton, S.W., Chu, X., Anbar, A.D., 2008. Tracing the stepwise oxygenation of the Proterozoic ocean. *Nature* 452, 456–459.

Shields, G., Stille, P., 2001. Diagenetic constraints on the use of cerium anomalies as palaeoseawater redox proxies: an isotopic and REE study of Cambrian phosphorites. *Chemical Geology* 175, 29–48.

Schulz, H.N., Brinkhoff, T., Ferdelman, T.G., Hernández Mariné, M., Teske, A., Jørgensen, B.B., 1999. Dense Populations of a Giant Sulfur Bacterium in Namibian Shelf Sediments. *Science* 286, 493–495.

Schulz, H.N., Schulz, H.D., 2005. Large sulfur bacteria and the formation of phosphorite. *Science* 307, 416–418.

Taylor, J.C., 1991. Computer programs for standardless quantitative analysis of minerals using the full powder diffraction profile. *Powder Diffraction* 6, 2–9.

Taylor, S.R., McLennan, S.M., 1985. The Continental Crust; Its composition and evolution: an examination of the geochemical record preserved in sedimentary rocks. 312 pp.

Trueman, C.N., 2013. Chemical taphonomy of biomineralized tissues. *Palaeontology* 56, 475–486.

Vitousek, P.M., Porder, S., Houlton, B.Z., Chadwick, OA., 2010. Terrestrial phosphorus limitation: mechanisms, implications, and nitrogen-phosphorus interactions. *Ecological applications* 20, 5–15.

Walker, R.J., Morgan, J.W., Hanski, E., Smolkin, V.F., 1997. Re–Os systematics of early Proterozoic ferropicrites, Pechenga Complex, NW Russia: evidence for ancient 187Os-enriched plumes. *Geochimica et Cosmochimica Acta 61*, 3145–3160.

Wright, J., Schrader, H., Holser, W.T., 1987. Paleoredox Variations in Ancient Oceans Recorded by Rare-Earth Elements in Fossil Apatite. *Geochimica et Cosmochimica Acta* 51, 631–644.

SUMMARY IN ESTONIAN

Apatiidi petrograafia ja haruldaste muldmetallide koostis 2 miljardi aasta vanustes Onega ja Petšenga basseinide setendites: fosfogeneesi paleokeskkonna rekonstrueerimine

Kuigi fosfori sisaldus maakoores on ainult 0.09% on fosfor bioevolutsiooniliselt võtmetähtsusega element, millel on oluline roll nii elu geneetilises koodis, kui ka organismide aine-energiavahetuses. Just viimasel põhjusel on fosfor olnud läbi geoloogilise ajaloo üks olulisemaid primaarproduktsiooni piiravaid elemente. Looduslikus fosforiringes kanduvad murenemisega kivimitest vabanevad fosforiühendid jõgedega maailmamerre, kus need kiiresti omastatakse biomassi kasvatamiseks. Fosfori eemaldumine veekogude veest toimub eelkõige läbi settimise, kas siis orgaanilise aine koosseisus või adsorbeerinult raua ja mangaani oksühüdroksiididega. Setteruumis toimub orgaanilisse aine lagunemisel või Fe-Mn faaside redutseerumisel fosfori vabanemine ja kontsentreerumine piirini kus on võimalik kaltsiumfosfaatse mineraali, apatiidi, kristalliseerumine ning fosfori-rikka sette (fosforiidi) moodustumine.

Tänapäevane fosfogenees ja kaasaegsete fosforiitide moodustumine toimub peamiselt mandrilava äärealadel, kus kerkehoovustega (nn *upwelling* hoovustega) transporditakse ookeani pinnakihtidesse fosfori ja lämmastikurikast süvaookeani vett, mis tingib nendes piirkondades kõrge primaarproduktsiooni, nagu see toimub näiteks Namiibia ja Peruu/Tšiili mandrilavadel. Apatiidi kristalliseerumismehhanismid nende alade põhjasetetes ei ole tänaseni üheselt selged, kuid kindlasti on selle esilekutsumiseks vaja protsesse, mis suudaksid sette pooriruumis kontsentreerida fosfaatset fosforit apatiidi üleküllastuseni.

Tüüpiliselt kujunevad apatiidi kristalliseerumiseks piisavad fosfaadi kontsentratsioonid settesisestel redokspiiridel, kus lahustunud fosfori kontsentreerumine saavutatakse Fe-Mn oksühüdroksiidide tsüklilise lahustumise-kristalliseerumisega ja samaaegse transpordiga üle muutuva asendiga redoksbarjääri või settesiseste (sulfaatiredutseerivate) bakterite metabolismiga kontrollitud primaarse orgaanilise ainese lagunemisprotsesside vahendusel. Seejuures on viimasel kümnendil üha enam hakanud levima arvamus, et settesisese lahustunud fosfaadi kontsentreerumisel mängivad olulist rolli väävlit oksüdeeruvad bakterid. Nimetatud bakterid (nt *Beggiatoa, Thiomargarita*), elavad ookeani põhjasetete ülemises, mõne cm paksuses osas, aeroobse ja anoksilise keskkonna piiril. Aeroobsetes tingimustes salvestavad bakterid oma rakkudes polüfosfaati ja nitraati. Keskkonnatingimuste muutumisel anoksilisteks kasutavad bakterid polüfosfaadi varusid energiaallikana ning vabastavad hüdrolüüsitud fosfaadi neid ümbritsevasse pooriruumi. Selle tulemusena suureneb lahustunud fosfaadi sisaldus üleküllastuseni, mis omakorda viib apatiidi väljasettimisele.

Ulatuslike setteliste fosfaatide tekkimine on peamiselt seotud Fanerosoikumiga, kuid esimesed fosfori-rikkad settekivimid ilmuvad geoloogilistes läbilõigetes juba Paleoproterosoikumis, ligikaudu kaks miljardit aastat tagasi.

Seejuures on tähelepanuväärne, et sarnase vanusega (umbes kaks miljardit aastat) fosforiite on leitud paljudest kohtadest üle maakera ning seetõttu võib arvata, et nende samaaegse moodustumise põhjustas mingi globaalne sündmus. Eelkõige on nende esimeste fosforiitide tekkimist seostatud Suure Hapniku Sündmusega, mis leidis aset umbes 2,3 miljardit aastat tagasi ning mille tulemusena tekkis Maa atmosfääri esmakordselt vaba hapnik. Selle tulemuseks oli Maa geo- ja biokeemiliste aineringete põhimõtteline ümberkorraldumine. Muuhulgas käivitus intensiivne oksüdatiivne murenemine. Just hapnikulise murenemise ilmumisega seostatakse fosfori sissekande suurenemist maailmamerre, primaarproduktsiooni intensiivistumist ja esimeste fosforiitide tekkimist. Samuti on oluline, et samal ajal koos atmosfääri hapnikustumisega sai võimalikuks ka merelise sulfaadireservuaari kujunemine ning sulfaat-sulfiidsete redoksbarjääride kujunemine.

Käesolevas doktoritöös uuriti ühtesid maailma vanimaid fosforiite, mis pärinevad kahest ligikaudu kahe miljardi aasta vanusest settebasseinist – Onega basseinist Karjalas ning Petšenga Rohekivimite vööndist Koola poolsaarel. Doktoritöö eesmärgiks oli selgitada keskkonnatingimused nende fosforiitide moodustuse ajal ning võrrelda neid tänapäevaste fosfogeneesikeskkondadega. Uuringute põhitähelepanu keskendus settelise apatiidi mikropetrograafiale ja koostisele, mille keskmes oli keskkonna redokstingimuste interpreteerimist võimaldavate haruldaste muldmetallide (lantanoidide) jaotumine ning sisaldused apatiidis.

Onega basseinis esinevad fosfori-rikkad setendid Zaonega kihistus kus peamine fosfori-mineraal apatiit esineb lamellide, läätsede ja konkretsioonidena, mis esinevad orgaanilise süsiniku rikkas mudakivimis. Lamellide, läätsede ja konkretsioonide elektronmikroskoopiline uuring näitas, et apatiit moodustab nendes erineva ümberkristalliseerumisastmega silindrilisi agregaate. Kõige parema säilivusega agregaadid koosnevad nanomeetri-suurustest apatiidi kristalliitidest, mis on läbipõimunud peendispersse orgaanilise süsinikuga ning mis võivad esindada fossiliseerunud (mineraliseerunud) mikroorganismide pseudomorfoose. Lantanoidide normaliseeritud sisaldused Zaonega kihistu kõige vähem ümberkristalliseerunud diageneetilises apatiidis näitavad nõrka negatiivset Ce ja tugevat positiivset Eu anomaaliat. Negatiivset Ce anomaaliat võib tõlgendada kui aeroobse sette- ja/või diageneesikeskkonna indikaatorit. Positiivne Eu anomaalia viitab aga tugevale hüdrotermaalsele mõjule apatiidi settimisel.

Erinevalt Onega basseini Zaonega kihistu setendites esinevast *in situ* settelisest apatiidist on Petšenga basseini Pilgujärvi settekihistu (*Pilgujärvi Sedimentary Formation*) apatiit ümbersettinud. Apatiit Pilgujärvi settekihistus esineb arvatavasti mandrilava nõlval paiknenud veealuse deltasüsteemi turbidiitsetes setendites liiva-kruusa terasuurusega fosfaatsete teradena, mis on tõenäoliselt pärinevad mandrilava äärealalt. Lähtuvalt fosfaatsete terade petrograafilisest ehitusest võib eristada nelja erinevat gruppi mida iseloomustavad mõnevõrra erinevad lantanoidide sisaldused. Erinevused petrograafiliste tüüpide lantanoidide spektrites on arvatavasti tingitud erinevatest varadiageneetilistest tingimustest apatiidi moodustumisel, aga mitte hilisematest settimisjärgsetest

hilisdiageneetilistest ja/või-moondeprotsessidest, sest erinevat tüüpi terad esinevad koos samades proovides. Juhul kui ümberkristalliseerumine oleks toimunud peale setendi moodustumist, peaksid kõikide terade lantanoidide spektrid olema ühesugused. Pilgujärvi settekihistus oli kõige parema säilivusega ning kõige enam tüüpilisele mereveele sarnase lantanoidide spektriga teradele iseloomulik, sarnaselt Onega basseini Zaonega kihistu diageneetilisele apatiidile, nõrk negatiivne Ce anomaalia ning samuti positiivne Eu anomaalia.

Seega võib järeldada, et mõlemas, nii Onega kui ka Petšenga basseinis, valitsesid apatiidi kristalliseerumisel merepõhja settekolonni ülemises osas sarnased anoksilised keskkonnatingimused, mis omakorda viitab, et tõenäoliselt kontrollisid apatiidi väljasettimist sarnased protsessid. Arvatavasti märgib apatiidi väljasettimise algust mõlemas basseinis spetsiifiliste anaeroobse (sulfiidse) – anoksilise redokspiiri moodustumist sette ülemises mõne cm paksuses osas. Samasugused redokstingimused on iseloomulikud piirkondadele, kus toimub kaasaegne fosfogenees. Mõlema basseini diageneetilist apatiiti iseloomustav positiivne Eu anomaalia viitab olulisele hüdrotermaalsete fluidide sissekandele fosforiidi settimise ajal, mis on kooskõlas nende basseinide tektooniliselt ja magmaliselt aktiivse iseloomuga, mida kinnitavad ka nende geoloogilises läbilõikes esinevad arvukad sillid ja laavavoolud.

ACKOWLEDGEMENTS

I am grateful to my supervisors Kalle Kirsimäe and Aivo Lepland whose help and guidance throughout my PhD studies is highly appreciated. I would like to thank all my co-authors for their help on the field, in the lab and during the writing process. Also all my colleagues and co-workers are gratefully acknowledged, especially everyone from the room 3005. Financial support from the Estonian Research Council (PUT969), Doctoral School of Earth Sciences and Ecology and Archimedes Foundation (Kristjan Jaak Scholarship) are gratefully acknowledged.

CURRICULUM VITAE

Name: Lauri Joosu
Date of birth: 19.08.1986
Address: Department of Geology, University of Tartu,
Ravila 14a, 50411 Tartu, Estonia
Contact: Phone +372 556 420 43
E- mail: lauri.joosu@ut.ee

Education

2010–…	University of Tartu, Department of Geology PhD student in Geology
2008–2010	University of Tartu, MSc in environmental technology
2005–2008	University of Tartu, BSc in environmental technology
2002–2005	Tartu Kivilinna Gümnaasium

Professional employment

2014– …	Applied Geologist, Eesti Energia AS
2012– 2014	Data analysis specialist, University of Tartu, Department of Geology
2007– 2010	Environmental expert, Miracon Grupp OÜ

Field of research:
geochemistry, minearology, phosphorus cycle, geobiology

Publications

1. Jonuks, T., **Joosu, L.**, (2013) Pendants of St. Anthony cross with the Crucifixion from Estonia – Possible Badges of a Folk Pilgrimage. *Estonian Journal of Archaeology* 17, 123– 138.
2. **Joosu, L.**, Lepland, A., Kirsimäe, K., Romashkin, A.E., Roberts, N.M.W., Martin, A.P., Črne, A.E., (2015) The REE-composition and petrography of apatite in 2 Ga Zaonega Formation, Russia: The environmental setting for phosphogenesis. *Chemical Geology* 395, 88–107.
3. Lepland, A., **Joosu, L.**, Kirsimäe, K., Prave, A.R., Romashkin, A.E., Crne, A.E., Martin, A.P., Fallick, A.E., Somelar, P., Upraus, K., Mand, K., Roberts, N.M.W., van Zuilen, M.A., Wirth, R., Schreiber, A., (2014) Potential influence of sulphur bacteria on Palaeoproterozoic phosphogenesis. *Nature Geoscience* 7, 20–24.
4. Lepland, A., Melezhik, V.A., Papineau, D., Romashkin, A.E., **Joosu, L.,** (2013). The earliest phosphorites: radical change in the phosphorus cycle during the Palaeoproterozoic. In: Melezhik, V.A., Prave, A.R., Hanski, E.J., Fallick, A.E.; Lepland, A., Kump, L. (Eds.). *Reading the Archive of Earth's Oxygenation*. Volume 3: *Global Events and the Fennoscandian Arctic Russia – Drilling Early Earth Project*. Springer, pp. 1275–1296.

5. **Joosu, L**., Lepland, A., Kreitsmann, T., Üpraus, K., Roberts, N.M.W., Paiste, P., Martin, A.P., Kirsimäe, K., (2015) Petrography and the REE-composition of apatite in the Paleoproterozoic Pilgujärvi Sedimentary Formation, Pechenga Greenstone Belt, Russia. Manuscript submitted to G*eochimica et Cosmochimica Acta*.

ELULOOKIRJELDUS

Nimi: Lauri Joosu
Sünniaeg: 19.08.1986
Aadress: Geoloogia osakond, Tartu Ülikool,
Ravila 14a, 50411 Tartu, Eesti
Kontakt: Tel. +372 5642043
E- post: lauri.joosu@ut.ee

Haridus

2010–…	Tartu Ülikool, Geoloogia osakond, Geoloogia doktorant
2008–2010	Tartu Ülikool, MSc keskkonnatehnoloogias
2005–2008	Tartu Ülikool, BSc keskkonnatehnoloogias
2002–2005	Tartu Kivilinna Gümnaasium

Teenistuskäik

2014– …	Rakendusgeoloog, Eesti Energia AS.
2012– 2014	Andmetöötlus spetsialist, Tartu Ülikool, Geoloogia osakond.
2007– 2010	Keskonnaekspert, Miracon Grupp OÜ.

Teadustöö põhisuunad:
geokeemia, mineraloogia, fosfori ringe, geobioloogia

Publikatsioonid

1. Jonuks, T., **Joosu, L.**, (2013) Pendants of St. Anthony cross with the Crucifixion from Estonia – Possible Badges of a Folk Pilgrimage. *Estonian Journal of Archaeology* 17, 123– 138.
2. **Joosu, L.**, Lepland, A., Kirsimäe, K., Romashkin, A.E., Roberts, N.M.W., Martin, A.P., Črne, A.E., (2015) The REE-composition and petrography of apatite in 2 Ga Zaonega Formation, Russia: The environmental setting for phosphogenesis. *Chemical Geology* 395, 88–107.
3. Lepland, A., **Joosu, L.**, Kirsimäe, K., Prave, A.R., Romashkin, A.E., Crne, A.E., Martin, A.P., Fallick, A.E., Somelar, P., Upraus, K., Mand, K., Roberts, N.M.W., van Zuilen, M.A., Wirth, R., Schreiber, A., (2014) Potential influence of sulphur bacteria on Palaeoproterozoic phosphogenesis. *Nature Geoscience* 7, 20–24.
4. Lepland, A., Melezhik, V.A., Papineau, D., Romashkin, A.E., **Joosu, L.,** (2013). The earliest phosphorites: radical change in the phosphorus cycle during the Palaeoproterozoic. In: Melezhik, V.A., Prave, A.R., Hanski, E.J., Fallick, A.E.; Lepland, A., Kump, L. (Eds.). *Reading the Archive of Earth's Oxygenation*. Volume 3: *Global Events and the Fennoscandian Arctic Russia – Drilling Early Earth Project*. Springer, pp. 1275–1296.
5. **Joosu, L**., Lepland, A., Kreitsmann, T., Üpraus, K., Roberts, N.M.W., Paiste, P., Martin, A.P., Kirsimäe, K., (2015) Petrography and the REE-

composition of apatite in the Paleoproterozoic Pilgujärvi Sedimentary Formation, Pechenga Greenstone Belt, Russia. Manuscript submitted to G*eochimica et Cosmochimica Acta*.

DISSERTATIONES GEOLOGICAE UNIVERSITATIS TARTUENSIS

1. **Пээп Мянник.** Конодонты в верхнеордовикских и нижнесилурийских отложениях Эстонии. Тарту, 1992, 355 с.
2. **Elvi Tavast.** Fennoskandia kilbi lõunanõlva ja sellega piirnevate alade aluspõhja reljeef. Tartu, 1992, 357 lk.
3. **Kaarel Orviku.** Characterisation and evolution of Estonian seashores. Tartu, 1992, 19 p.
4. **Анатолий Молодьков.** ЭПР-анализ скелетного вещества моллюсков в хроностратиграфических исследованиях позднего кайнозоя. Тарту, 1992, 33 с.
5. **Jaan Lutt.** Late- and postglacial deposits on the Estonian shelf. Tartu, 1993, 31 p.
6. **Reet Karukäpp.** Gotiglatsiaalne morfogenees Skandinaavia mandriliustiku kagusektoris. Tartu, 1997, 181 p.
7. **Argo Jõeleht.** Geothermal studies of the Precambrian basement and Phanerozoic sedimentary cover in Estonia and Finland. Tartu, 1998, 125 p.
8. **Jüri Nemliher.** Mineralogy of Phanerozoic skeletal and sedimentary apatites: an XRD study. Tartu, 1999, 134 p.
9. **Kalle Kirsimäe.** Clay mineral diagenesis on the Lower Cambrian "Blue Clay" in the northern part of the Baltic Paleobasin. Tartu, 1999, 113 p.
10. **Jüri Plado.** Gravity and magnetic signatures of meteorite impact structures. Tartu, 2000, 87 p.
11. **Olev Vinn.** Morphogenesis and phylogenetic relationships of Clitambonitidines, Ordovician Brachiopods. Tartu, 2001, 127 p.
12. **Leho Ainsaar.** The middle Caradoc facies and faunal turnover in the late Ordovician Baltoscandian palaeobasin: sedimentological and carbon isotope aspects. Tartu, 2001, 109 p.
13. **Oive Tinn.** Early Ostracode evolution and Palaeoenvironmental application in the Ordovician of Baltoscandia. Tartu, 2002, 145 p.
14. **Maris Rattas.** Subglacial environments in the formation of drumlins – The case of the Saadjärve Drumlin Field, Estonia. Tartu, 2004, 117 p.
15. **Ene Kadastik.** Upper-Pleistocene stratigraphy and deglaciation history in northwestern Estonia. Tartu, 2004, 129 p.
16. **Helje Pärnaste.** Early Ordovician trilobites of suborder Cheirurina in Estonia and NW Russia: systematics, evolution and distribution. Tartu, 2004, 138 p.
17. **Mari-Ann Mõtus.** Silurian (Llandovery-Wenlock) tabulate corals of Baltoscandia: taxonomy, palaeoecology, distribution. Tartu, 2005, 167 p.
18. **Alar Rosentau**. Development of proglacial lakes in Estonia. Tartu, 2006, 114 p.
19. **Evelin Verš.** Development of impact-induced hydrothermal system at Kärdla impact structure. Tartu, 2006, 96 p.
20. **Sigitas Radzevičius.** The genus *Pristiograptus* in wenlock of East Baltic and the Holy Cross Mountains. Tartu, 2007, 133 p.
21. **Andres Marandi.** Natural chemical composition of groundwater as a basis for groundwater management in the Cambrian-Vendian aquifer system in Estonia. Tartu, 2007, 116 p.
22. **Eve Niinemets.** Vegetation and land-use history of the Haanja Heights (SE-Estonia) during the holocene. Tartu, 2008, 146 p.

23. **Kalle-Mart Suuroja.** Geology and lithology of the early palaeozoic marine impact stuctures kärdla and neugrund (estonia). Tartu, 2008, 234 p.
24. **Rutt Hints.** Early diagenesis of Ordovician and Silurian Bentonites in the Northern Baltic Palaeobasin. Tartu, 2009, 90 p.
25. **Peeter Somelar.** Illitization of K-bentonites in the Baltic Basin. Tartu, 2009, 118 p.
26. **Ulla Preeden.** Remagnetizations in sedimentary rocks of Estonia and shear and fault zone rocks of southern Finland. Tartu, 2009, 121 p.
27. **Kati Tänavsuu-Milkeviciene.** Transgressive to regressive turnaround in the Middle Devonian Baltic Basin. Tartu, 2009, 106 p.
28. **Valle Raidla.** Chemical and isotope evolution of groundwater in the Cambrian-Vendian aquifer system in Estonia. Tartu, 2010, 134 p.
29. **Kadri Sohar.** Quaternary ostracods from Estonia and their application in palaeo-environmental reconstruction. Tartu, 2010, 140 p.
30. **Kristjan Urtson.** Stepwise melt transport and accumulation: analogue and numerical modelling approach. Tartu, 2011, 83 p.
31. **Marko Kohv.** Landslides in clayey soils of western Estonia. Tartu, 2011, 116 p.
32. **Nele Muttik.** Post-impact alteration of impactites: Ries crater, Germany. Tartu, 2011, 78 p.
33. **Annette Sedman.** Strength and self-cementing properties of oil shale retorting wastes. Tartu, 2013, 82 p.
34. **Arkady Tsyrulnikov.** Complex seismo-acoustic and lithological study of the Lateglacial and postglacial sediments northern Gulf of Riga, eastern branch of the central Baltic Sea. Tartu, 2013, 102 p.
35. **Marge Uppin.** Geological sources and hydrochemistry of fluoride and boron in Silurian-Ordovician aquifer system. Tartu, 2013, 86 p.
36. **Peeter Talviste**. Temporal changes in weak natural and artificial soils – influence on geotechnical characteristics. Tartu, 2014, 204 p.
37. **Katrin Lasberg.** Chronology of the Weichselian Glaciation in the southeastern sector of the Scandinavian Ice Sheet. Tartu, 2014, 100 p.
38. **Sirle Liivamägi**. Neoproterozoic Baltic paleosol: geology and paleoenvironmental interpretation. Tartu, 2015, 94 p.